Design Optimization of Plate Heat Exchanger by Utilizing Artificial Intelligence

by

Seyit Ahmet Kuzucanlı

A Dissertation Submitted to the
Graduate School of Health Sciences
in Partial Fulfillment of the Requirements for
the Degree of

Master of Science

in

Mechanical Engineering

KOÇ
ÜNİVERSİTESİ

August 9th, 2023

Design Optimization of Plate Heat Exchanger by Utilizing Artificial Intelligence

Koç University

Graduate School of Sciences and Engineering

This is to certify that I have examined this copy of a master's thesis by

Seyit Ahmet Kuzucanlı

and have found that it is complete and satisfactory in all respects,

and that any and all revisions required by the final

examining committee have been made.

Committee Members:

Prof. Demircan Canadinç (Advisor)

Prof. Murat Sözer

Assist. Prof. S. Mine Toker

Date: August 9th, 2023

Dedicated to my family.

ABSTRACT

Design Optimization of Plate Heat Exchanger by Utilizing Artificial Intelligence

Seyit Ahmet Kuzucanlı

Master of Science in Mechanical Engineering

August 9th, 2023

The plate heat exchangers are components that provide heat transfer between two or more mediums; therefore, they have crucial importance in the industry. While the plate heat exchangers are produced, sheet metal forming process is employed. Growing interest in manufacturing lightweight, cost effective, and robust products in HVACR industry motivates the search for compact plate heat exchangers used in combi-boilers. Lightweight compact plate heat exchangers distinguish them from other plate heat exchangers in case of raw materials shortage periods. However, manufacturing lightweight plate heat exchangers requires time consuming simulation works and significant investment for production trials. On the other hand, implementation of machine learning assisted optimization process has been proved promising and reasonable alternative for traditional production methods which inspired current work: “design optimization of plate heat exchangers by utilizing artificial intelligence” that satisfies requirements stated in material order specifications of Bosch Home Comfort.

In this work, an extensive dataset was constructed from finite element analysis simulations on sheet metal forming process by considering the design limits of compact plate heat exchanger produced in Bosch Home Comfort Manisa Plant to train multilayer feed-forward neural network algorithm. The maximum thinning amount of metal plates after forming process was predicted by using optimized neural network algorithm. Six cases with desired outputs were selected to validate neural network algorithm predictions. The demonstrated thinning amounts verify the success of machine learning algorithm in design optimization of plate heat exchangers.

ÖZETÇE

Yapay Zeka Kullanarak Plakalı Eşanjörlerin Tasarım Optimizasyonu

Seyit Ahmet Kuzucanlı

Makine Mühendisliği, Yüksek Lisans

Ağustos 9, 2023

Plakalı eşanjörler, iki veya daha fazla ortam arasında ısı transferini sağlayan; bu nedenle endüstride çok önemli bir öneme sahiptirler. Plakalı eşanjörler üretilirken sac şekillendirme işlemi uygulanmaktadır. HVACR endüstrisinde hafif, uygun maliyetli ve sağlam ürünler üretmeye yönelik artan ilgi, kombilerde kullanılan kompakt plakalı ısı eşanjörleri arayışını motive ediyor. Hafif kompakt plakalı eşanjörler, hammadde sıkıntısı dönemlerinde onları diğer plakalı eşanjörlerden ayırır. Bununla birlikte, hafif plakalı ısı eşanjörlerinin üretimi, zaman alıcı simülasyon çalışmaları ve üretim denemeleri için önemli yatırımlar gerektirir. Öte yandan, makine öğrenimi destekli optimizasyon sürecinin uygulanmasının, Bosch Home Comfort'un malzeme siparişi spesifikasyonlarında belirtilen gereksinimleri karşılayan, mevcut çalışmaya ilham veren geleneksel üretim yöntemleri için umut verici ve makul bir alternatif olduğu kanıtlanmıştır.

Bu çalışmada, çok katmanlı ileri beslemeli sinir ağı algoritmasını eğitmek için Bosch Home Comfort Manisa fabrikasında üretilen kompakt plakalı ısı eşanjörünün tasarım limitleri göz önünde bulundurularak sac metal şekillendirme prosesinde sonlu elemanlar analizi simülasyonlarından kapsamlı bir veri seti oluşturulmuştur. Şekillendirme işleminden sonra metal plakaların maksimum incelme miktarı, optimize edilmiş sinir ağı algoritması kullanılarak tahmin edildi. Sinir ağı algoritması tahminlerini doğrulamak için istenen çıktılara sahip altı durum seçildi. Gösterilen inceltme miktarları, makine öğrenme algoritmasının plakalı ısı eşanjörlerinin tasarım optimizasyonundaki başarısını doğrulamaktadır.

ACKNOWLEDGEMENTS

I would like to express my deepest gratitude to my advisor, Prof. Demircan Canadinç, for his invaluable guidance and support throughout my master's program. He has been a great mentor and a source of inspiration for me. His expertise and patience have played a crucial role in the success of this thesis. I would also like to thank Prof. Murat Sözer and Asst. Prof. S. Mine Toker for serving in my thesis committee and providing helpful feedback and suggestions. Their insights and comments have greatly improved the quality of this work.

I am grateful to Bosch Home Comfort for providing me with the opportunity to conduct my research and for all the resources and support they provided. I would also like to thank my colleagues at Bosch Home Comfort for their support and collaboration during my research. In particular, I would like to thank Berkay Türkcan İmrağ for his help while conducting simulations. He has been a valuable partner and a friend throughout this process.

I would like to extend my sincere gratitude to my friends Alp Emre Yaşar, Çağatay Kök, Sanem Ayaz Kök and Yiğit Gürler for their support. Their willingness to share their experiences and insights has been invaluable to my research. Thank you for your time and contribution.

Finally, I appreciate my parents, and my brother, Özgür Kuzucanlı and my fiancé, İpek Tanşuli, for their encouragement. Without your support, this thesis would not have been possible. You have been my motivation and strength in this journey.

TABLE OF CONTENTS

LIST OF TABLES

LIST OF FIGURES

ABBREVIATIONS

PHE	Plate Heat Exchanger
C-PHE	Compact Plate Heat Exchanger
HVACR	Heating, Ventilating, Air Conditioning, and Refrigeration
RMSE	Root Mean Squared Error
FEA	Finite Element Analysis
SMF	Sheet Metal Forming
ML	Machine Learning
ANN	Artificial Neural Network
AI	Artificial Intelligence
IP	Intellectual Property
SS	Stainless Steel
DOE	Design of Experiment
PCA	Principal Component Analysis

Chapter 1:
INTRODUCTION

1.1 Motivation

In this era, efficient use of material resources and lightweight design play a crucial role in the commercial success of all industries. Based on requirements, forming technologies provide different solutions for a wide range of component production made of various materials. The combination of increased strength with minimization of thickness and hence lightweight of components as well as minimal material usage achieves today's demands in a wide range of industries. Therefore, a constant increase in market share is observed in formed parts [1].

One can rely on advanced technologies like deep-drawing processes for the manufacturing of sheet metal parts. However, in terms of economics, these methods are often used for mass production because of large plant investments coupled with the high cost of custom-built tools, which are only used for a particular part shape. Small to medium batch components are needed in some industries, as the fabrication of plate heat exchangers, even though they are challenging to produce using traditional forming techniques [2].

Plate heat exchangers (PHEs) have been widely used in the heating, ventilating, air conditioning, and refrigeration (HVACR) industry due to their virtue of high thermal effectiveness and compactness. In heating appliances such as combi-boilers, mostly brazed PHEs are used due to the advantage of their small size. However, there are several difficulties during the production of PHEs such as formability, brazeability, and availability of raw material. These handicaps drive the HVACR industry to investigate alternative designs that could eliminate the forenamed disadvantages of PHEs. Besides compactness and high thermal effectiveness of compact brazed PHEs (C-PHE), as shown in Figure 1.1, C-PHE has unique pattern design that increases effective heat transfer surface area.

Figure 1.1. The chevron type compact brazed plate heat exchanger (C-PHE).
(Source: Bosch Home Comfort, 2023)

1.2 Background

The background information in this part includes details about PHEs, metal forming, finite element analysis (FEA) simulations, and machine learning. It is noteworthy that the emphasis is placed on PHEs, their characteristics, application areas, benefits and drawbacks, and the factors that affect PHEs. Furthermore, in-depth analysis is also made on the metal forming, FEA simulations, and machine learning models. Eventually, the implementation of machine learning algorithms in mechanical engineering is emphasized, and previous studies in this field are interpreted.

1.2.1 Plate Heat Exchangers

Heat exchangers are thermal devices that are used for heat transfer between two or more fluids, or between fluid and a solid surface in thermal contact at different temperatures [3]. There are typical applications of heat exchangers involving heating or cooling of targeted fluid stream in the HVACR industry, steam power plants, household refrigerators, and radiators [4]. PHEs are a particular class of heat exchangers that excel in industrial applications due to their various benefits such as high thermal effectiveness, lower costs compared to other existing heat exchanger options, and their relatively small sizes [5]. Chevron-type PHEs are among the most popular types of plate heat exchangers because of their superior thermal efficiency and lower pressure drop performance. Geometry of the chevron type plate heat exchanger is represented in Figure 1.2.

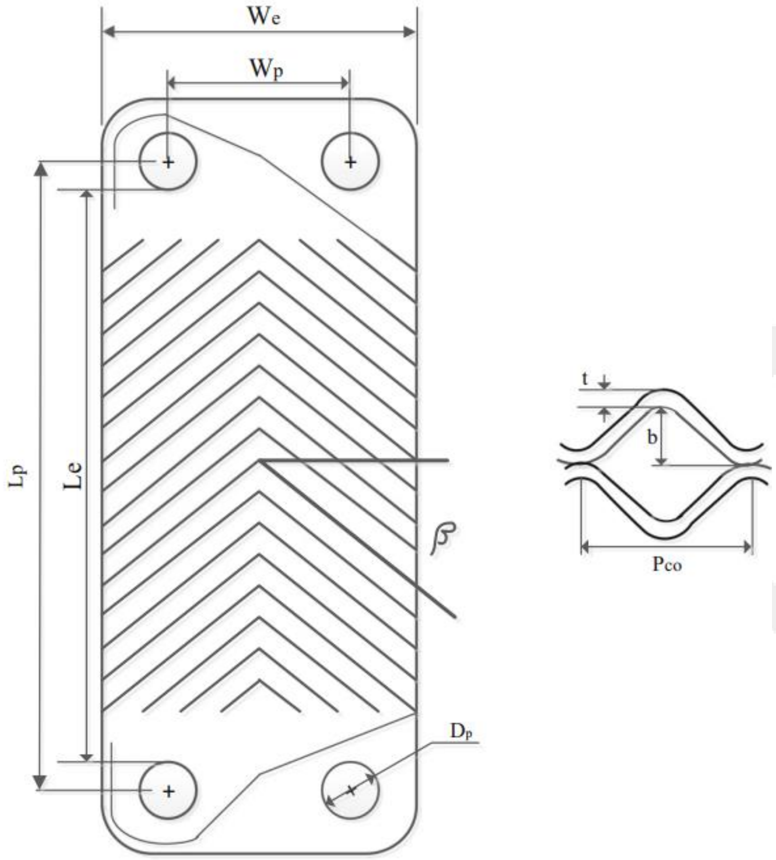

Figure 1.2. The geometry of the plate heat exchanger [6].

The design parameters illustrated in the figure above are listed in Table 1.1.

Table 1.1. Design parameters of the plate heat exchanger.

Symbol	Parameter
β	Chevron angle
b	Plate spacing
t	Plate thickness
P_{co}	Corrugation pitch
W_e	Effective width

PHEs typically consist of a stack of contacting corrugated steel plates in a frame. These plates have angles -also known as Chevron angles- to adjust heat transfer rate. There are three types of PHEs: gasketed, welded, and brazed. Vacuum brazed PHE has resistance for high thermal and pressure loads due to this reason it is suitable for combi-boiler applications. It is made by using two end plates (top and bottom), stainless steel plates, and braze filler material. In vacuum brazed PHEs, copper (Cu) is mostly employed as braze filler material [7].

1.2.2 Sheet Metal Forming

Sheet metal forming (SMF) is a highly complicated manufacturing process that is commonly used in the industry. In the SMF process, metal sheets are shaped in a desired direction by plastically deformed. Typically, the forming tools which consist of a blank holder, a punch, and a die are employed for the plastic deformation of metal sheets as shown in Figure 1.3.

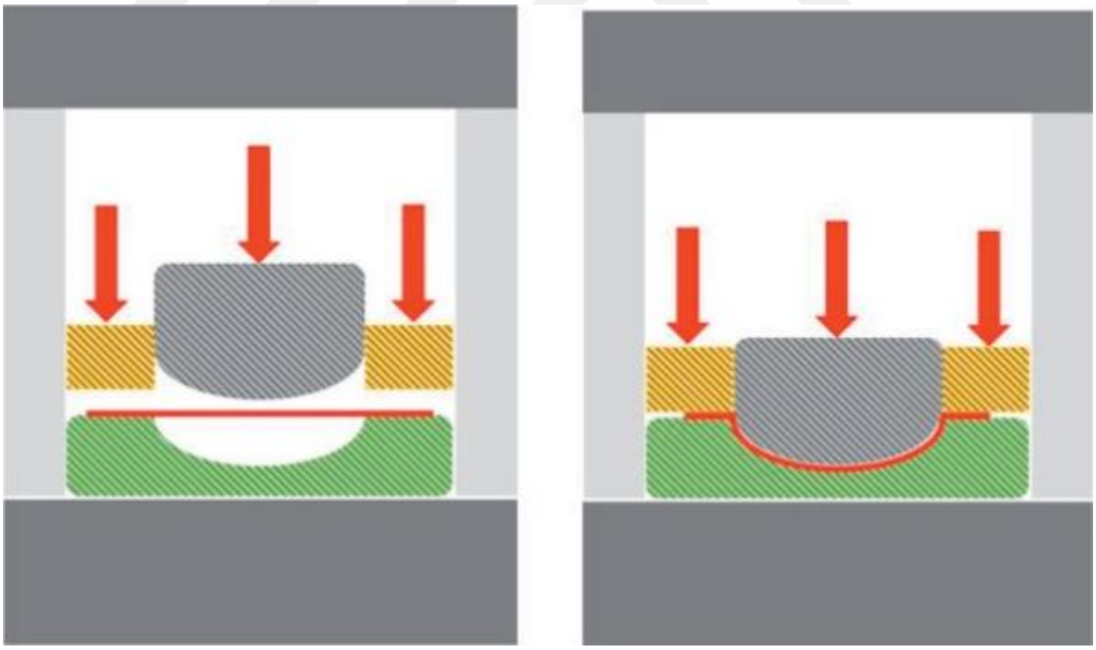

Figure 1.3. Representation of the SMF process [8].

Throughout the SMF process, a blank is placed over the die, and then it is pressed by the punch to create plastic deformation with the aim of obtaining desired shape. The versatility of mechanical properties, tool geometry, and process parameters makes formed components frequently prone to flaws like wrinkling, tearing, excessive thinning, and springback. In general, sheet metal forming processes enable the production of high quality components with high cadence and low cost [9].

Due to the numerous variables involved in the process, it can be very challenging to anticipate where and when these defects will occur. They can appear during any stage of the forming process. High quality and robustness standards have been demanded due to the ever-increasing competition in the HVACR industry. Furthermore, SMF is imperative to locate substitute sheet metal raw material sources for Bosch Home Comfort to deal with today's raw material availability issues.

1.2.3 FEA Simulations

In recent years, numerical simulation of sheet metal forming has developed into a crucial instrument for evaluating the deep drawing process's manufacturing viability and the initial designs of new stamped parts with complex 3D geometry. FEA simulations offer a low-cost alternative to conventional experiments in case optimization of design and process parameters [10]. The benefit of FEA is that it can anticipate part flaws like spring-back, rupture, wrinkling, buckling, and shape errors while also optimizing the process parameters [11].

The basic process flow of FEA simulations is presented in Figure 1.4. Basically, two major phases exist in the FEA process. The first part is related to the design process including objective, constraints, and design variables. These three items are strictly related to each other. The second part consists of solving process by using FEA software.

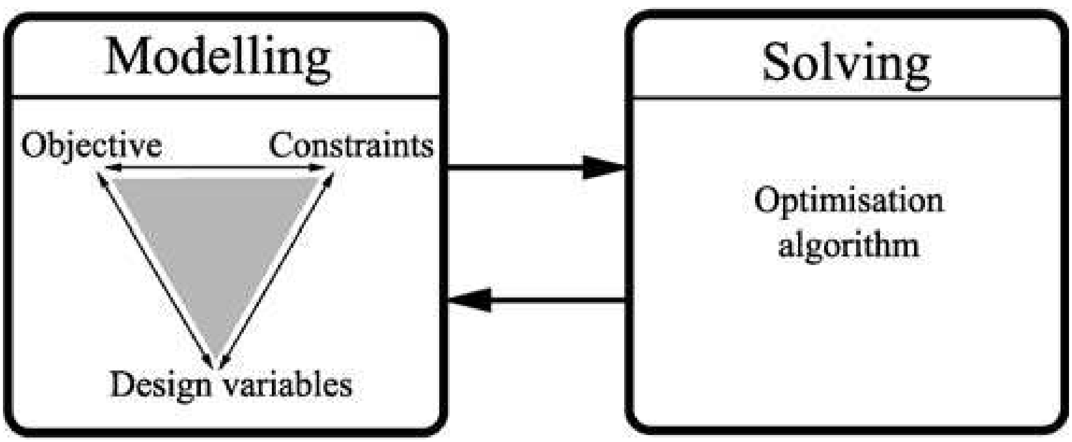

Figure 1.4. The basic process flow of FEA simulations [12].

FEA simulations start with modelling the problem by determining design variables, quantifying objective function, and constraints as shown in Figure 1.5.

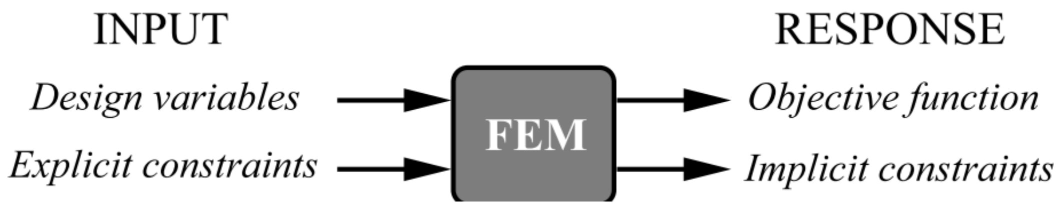

Figure 1.5 The FEA process model as input-response [13].

1.2.4 Machine Learning

Artificial intelligence (AI) is the science of building computational algorithms and systems able to imitate intelligent behavior of human [14]. The sophisticated tasks like learning, decision making, interpretation and perception can be performed by utilizing the computational systems and developed algorithms for a given problem [15]. Machine learning (ML) is one of the most known artificial intelligence applications dealing with enabling computer programs to improve their performance with experience obtained from learning process at certain tasks [16]. ML is the training of computers to optimize a performance criterion using example or prior data. A ML model is specified by a set of parameters, and the learning phase is running a computer to improve those parameters based on prior knowledge or training data [17]. The model may be descriptive to learn from data or predictive to make future predictions, or it may be both. There are two types of machine learning techniques: supervised, and unsupervised learning [18]. The ML approaches are described below and represented in Figure 1.6.

Classification (supervised learning) is known as a method to categorize objects based on characteristics of object [19].

Regression (supervised learning) is a mathematical technique for assessing the strength and nature of the relationship between the dependent variable and several other factors [20].

Clustering (unsupervised learning) lacks specified classifications as opposed to classification. Large datasets are clustered by dividing them into small, distinct subgroups or clusters. The Clustering method is employed to determine and categorize commonalities between locations [21].

Optimization and optimized AI models (supervised and unsupervised machine learning) are used in evolutionary computing, a branch of computer science that applies ideas from biological evolution to the solution of challenging issues [22].

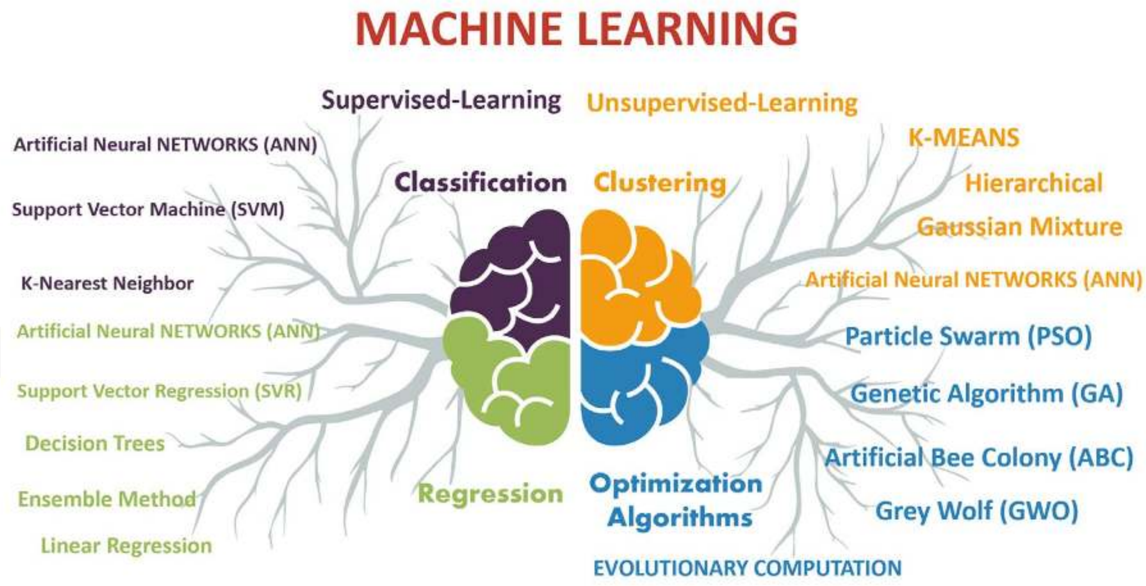

Figure 1.6. ML and optimization algorithms [23].

ANNs are designed by inspiring human brain, which are frequently utilized to comprehend complicated issues and generate logical answers using functional relationships [24]. In the analysis of non-linear processes with different effective parameters, ANNs would be appropriate method to employ. Architecture of ANN with single hidden layer is visually shown in Figure 1.7. The methodology of developing an ANN model is entirely based on trial-and-error method. In a typical ANN model, 80% of collected data are dedicated to train model, and the remaining part is used for testing and evaluating developed structures [25]. The performance of developed model is measured by using mean square error performance function (MSE). Using the MSE, the error between the ANN output and experimental output is calculated by following equation [26].

$$MSE = \frac{\sum_{i=1}^{n}\left(y_i-\lambda(x_i)\right)^2}{n} \quad (1.1)$$

where, y_i is the experimental value for the instance x_i, $\lambda(x_i)$ is the predicted value for the instance x_i, and n is the number of instances [27].

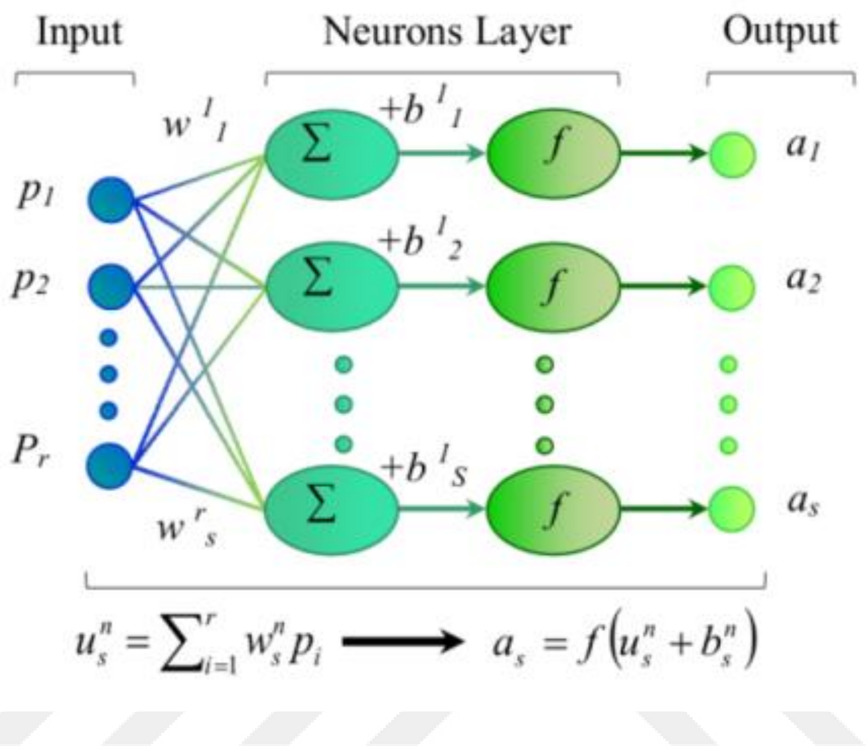

Figure 1.7. Schematic of the ANN with one hidden layer considering the weight matrices w, bias vectors b, linear combiner u and transfer function f [25].

1.3 Objective

Plentiful research area in mechanical engineering and the rising propensity for design optimization motivated researchers to come up with a new methodology. Due to ML's capability for prediction with previously unexplored inputs, its utilization in the design optimization process has drawn significant interest. The application of ML not only enables time and resource savings but also comprehensive research on the relevant field due to the necessity of data collection.

Recent studies on ML integrated design optimization in the field of engineering have proven capacity in SMF [28]–[36]. This study particularly focuses on work on the SMF process, where ML models are developed by coupling models with material information such as mechanical properties, chemical composition, and design parameters. The successful results of the research show a new approach to successful design without consuming more time and resources.

In this context, the demand for alternative raw materials of sheet metal for the production of PHEs in the HVACR industry and the aforementioned examples of successfully applied ML algorithms on optimization of SMF processes encouraged us to combine these two areas. In the current work, the main objective is to use ML algorithms to design a C-PHE with appropriate parameters to fulfil the reliability requirements of Bosch HC under thermal and pressure loads throughout its life cycle.

1.4 Delimitations

i. The production trial could not be planned due to the production plan of the Bosch Home Comfort Manisa Plant.

ii. The springback phenomena was excluded from the design optimization process.

iii. The type of the raw material was limited to 316L SS and 304L SS due to unavailability of alternative raw material in the market.

iv. Geometry wise evaluation and restriction due to IP protection of the C-PHE pattern design.

Chapter 2:
Material and Methods

2.1 *Design and Production Processes of C-PHE*

Plate heat exchangers is a component that is used for heat transfer between two or more working fluids by plates. Plates are formed according to certain patterns to increase heat transfer effectiveness of PHEs. Whereas there are various types of plate patterns, the most common pattern is chevron type plate patterns as shown in Figure 2.1. Besides heat transfer effectiveness, chevron patterned plate design is shaped based on operational loads such as thermal and pressure loads. In C-PHEs, copper brazing between steel plates is used to seal surfaces to mix two fluid mediums and to increase conductive surface to enhance heat transfer rate.

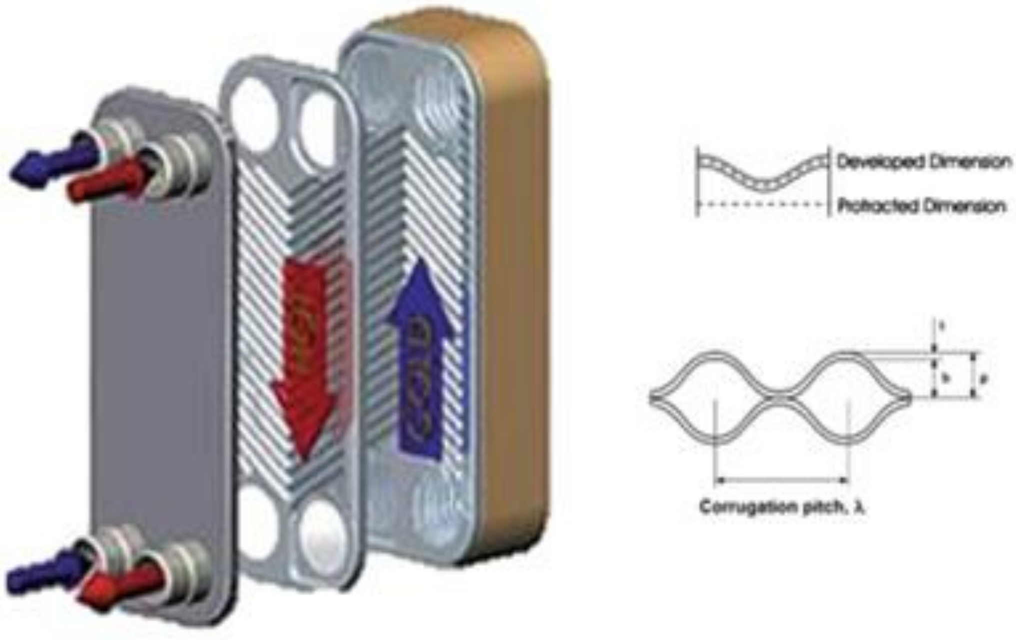

Figure 2.1. The compact brazed plate heat exchanger—construction (left) and parameters (right) [37].

The production process of C-PHE is listed below in Figure 2.2.

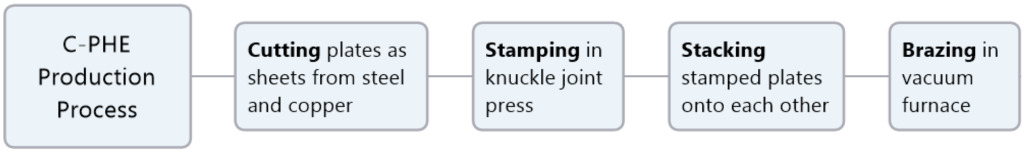

Figure 2.2. The production process of C-PHE in Bosch Home Comfort

The production process is initiated by cutting rolled stainless steel sheets according to determined size. After cutting plates, the stamping process takes place in C-PHEs production. In the stamping process, there are four elements employed; punch, blank holder, blank, and bed die as presented in Figure 2.3.

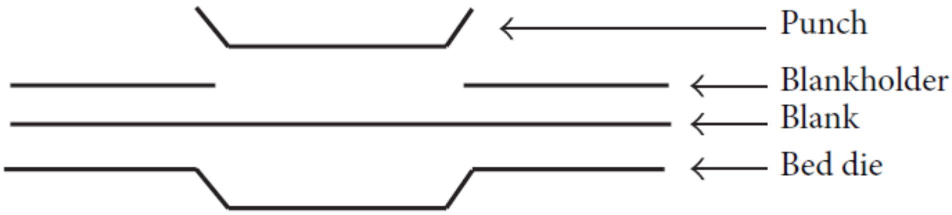

Figure 2.3. Elements of the stamping process.

The stamped plates and copper fillers are stacked onto each other as shown in Figure 2.4. Then, the stacked parts are conditioned to vacuum brazing furnace. The vacuum furnace operates at 1150 °C.

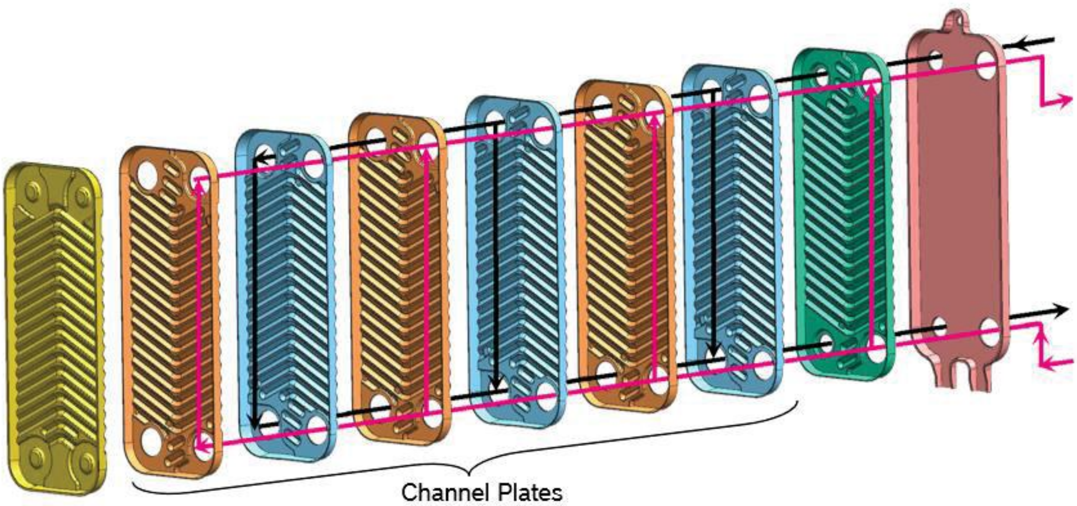

Figure 2.4. The stacking process of plates in the opposite chevron directions.

2.2 *Materials*

The C-PHE investigated in the current study was initially made of austenitic stainless-steel (SS) plates coupled with copper (Cu) as a braze filler material counterparts stacked together in a sandwich structure. It is important to consider that C-PHE consists of only SS plates. Copper acts as a braze filler material, and it completely melts at 1150 °C for 7-8 hours during heat treatment process in vacuum brazing furnace. After this process, final product as C-PHE is ready to assemble in combi-boiler as represented in Figure 2.4 [38].

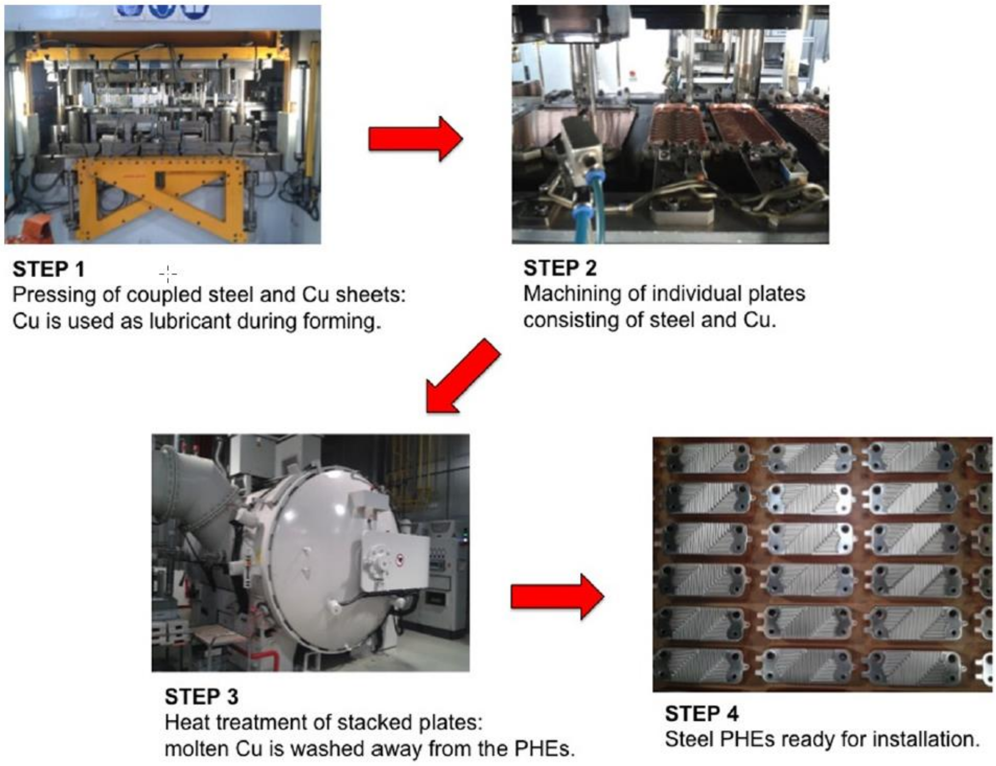

Figure 2.5. Schematic of the production process of the C-PHE [38].

The alternative raw materials for C-PHE plates are determined as the 316L SS and 304L SS in the current study. The chemical compositions of the 316L and 304L retrieved from Aperam are listed in Table 2.1, and Table 2.2 accordingly.

Table 2.1. Chemical composition of the 316L

Elements (%)	C	Si	Mn	Cr	Ni	Mo
316L	0.025	0.40	1.20	16.80	10.10	2.10

Table 2.2. Chemical composition of the 304L SS.

Elements (%)	C	Si	Mn	Cr	Ni
304L	0.025	0.40	1.40	18.20	8.05

2.3 *Material Characterization Tests*

The specimens of AISI 316L SS and AISI 304L SS were prepared for uniaxial tensile test, and hydraulic bulge test by complying with ASTM E8 | E8M standard [39]. Dimension and shape of test specimens are shown in Figure 2.6. The experiments were conducted by Atilim University, 2015 for the 316L SS, and FKA GmbH, 2022 for the 304L SS.

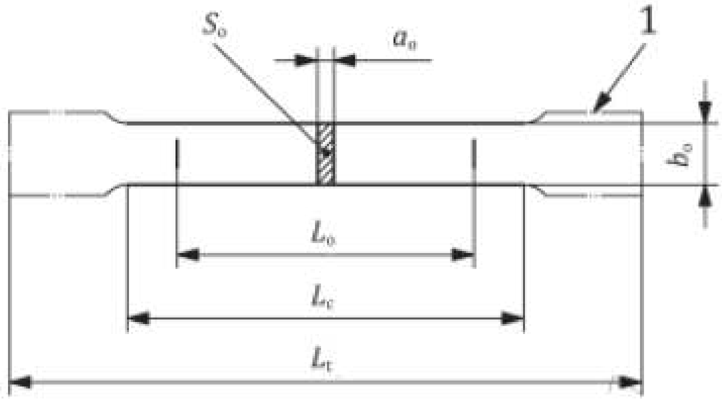

Test piece type	Width b_0	Original gauge length L_0	Parallel length L_c Minimum	Parallel length L_c Recommended	Free length between the grips for parallel sided test piece
1	12,5 ± 1	50	57	75	87,5

Figure 2.6. Shape and dimensions of the uniaxial tensile test specimens. (Source: Bosch Home Comfort)

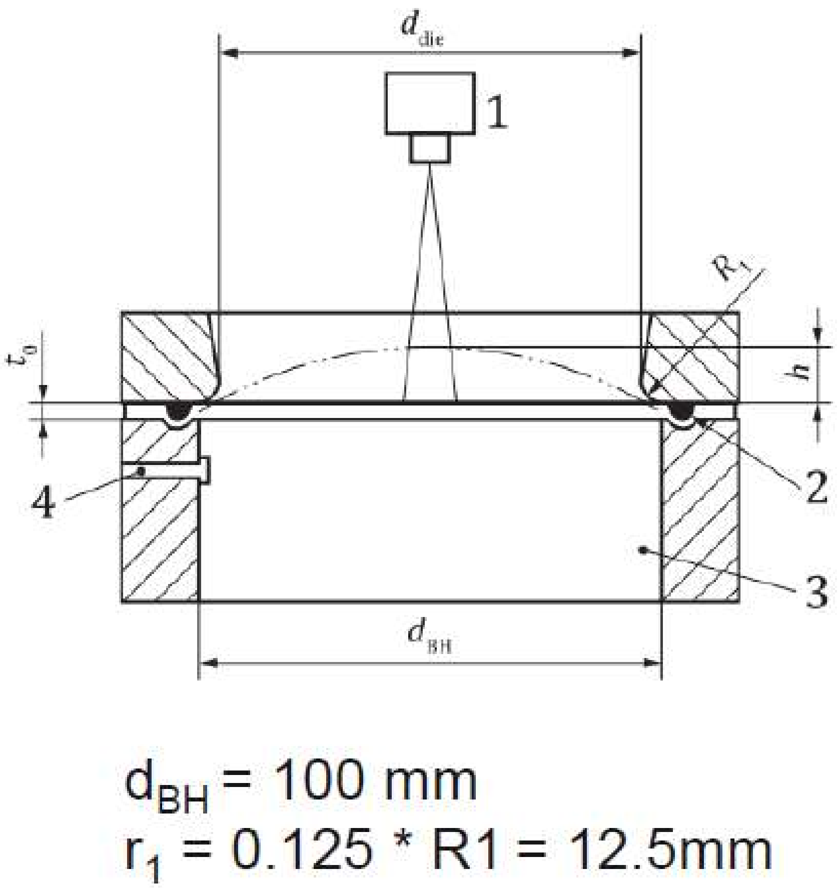

Figure 2.7. Shape and dimensions of the hydraulic bulge test specimens.

The uniaxial tensile tests were conducted with 5 probes to obtain engineering stress and strain curves while hydraulic bulge tests were conducted to gather yield stress curves. Consequently, the material card was created by utilizing the uniaxial tensile tests and the hydraulic bulge tests for the material 316L SS, and 304L SS.

2.4 *Finite Element Simulation*

Finite element methods have been broadly employed to optimize numerous sheet metal forming operations in order to prevent facing defects in production. Sheet metal forming is a highly complicated manufacturing process that is commonly used in industry. Considering the complexity of SMF process, trial and error method takes a lot of time. And tool revision is required when expected results are not achieved. Hence, employing trial and error method is expensive and time consuming [40]. To prevail over this problem, finite element method integrated computer simulations have been introduced.

There are many commercial FEA integrated simulations available for sheet metal forming including LS Dyna, ABAQUS, Nike 2D, Dynaform, etc. LS-Dyna version 4.8.29 is employed to simulate the present work. It is a non-linear dynamic FEA integrated simulation package which allows to simulate numerous types of sheet metal production process such as bending, deep drawing, stretching, etc. by including prediction of stress, strain and thickness distributions [41].

The models of the punch, the lower die, the blank holder, and the blank were constructed in LS-Dyna pre-processor according to the Bosch Home Comfort standards as shown in Figure 2.8.

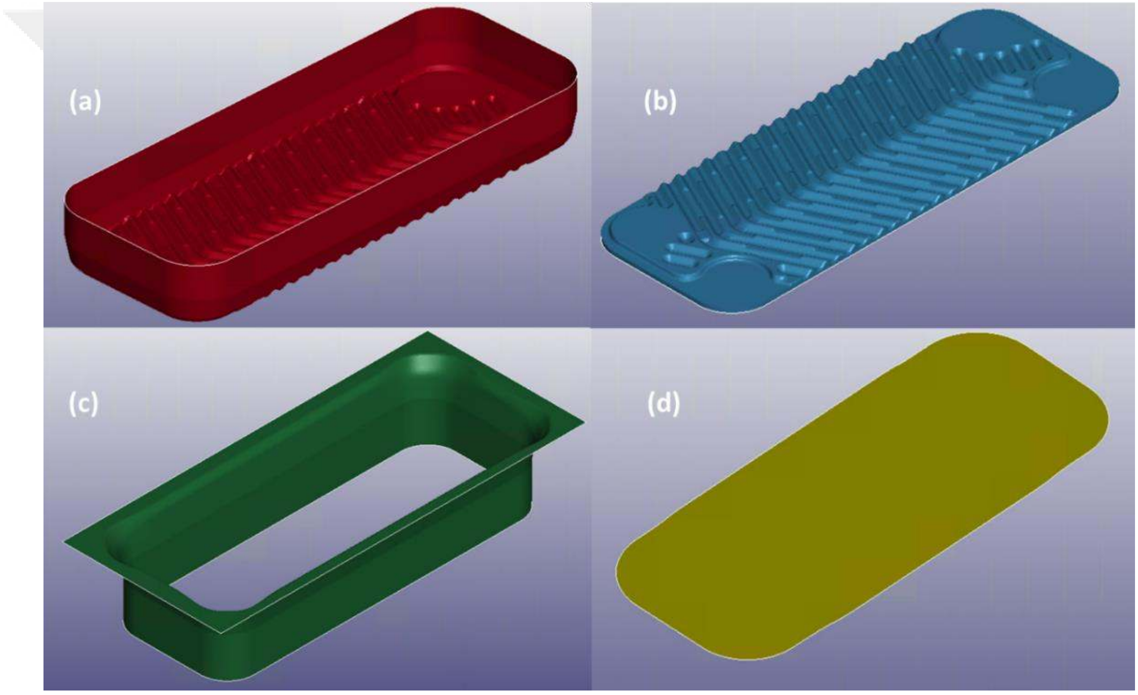

Figure 2.8. Components of the forming process in the C-PHE production; (a) the punch, (b) the die, (c) the blank holder, and (d) the blank.

2.4.1 Material Modeling

Over the years, the yield functions have been developed to characterize the plastic anisotropy of sheet metals by Hill, Barlat, and Banabic [42]–[44]. The above-mentioned yield functions have been implemented on LS Dyna to simulate the SMF processes. Sheet metals typically show a significant anisotropy of mechanical properties because of their crystalline structure and the peculiarities of the rolling process [44]. Successful SMF process simulations have been performed by making reasonable assumptions, although there are still some theoretical issues related to the distortion and rotation of the anisotropic reference frame [42].

Hill48 was the first anisotropic yield function evaluated in C-PHE SMF simulation process. Hill48 functions simply consists of explicit formulas with simple formulation and its coefficients. Hence, it takes place in literature as the quadratic criterion [45]. However, Hill48 yield function based SMF simulations cannot predict the plastic strain ratios and directional yield stress accurately. Due to drawbacks of the quadratic criterion, YLD2000 yield function proposed by Barlat has been evaluated.

The non-quadratic yield function proposed by Barlat et al. is represented as below two convex functions.

$$\phi(\sigma) = \phi' + \phi'' = 2\bar{\sigma}^a \tag{2.1}$$

$$\phi' = \left|\tilde{S}_1' - \tilde{S}_2'\right|^a, \text{ and } \phi'' = \left|2\tilde{S}_2'' + \tilde{S}_1''\right|^a + \left|2\tilde{S}_1'' + \tilde{S}_2''\right|^a \tag{2.2}$$

Components of above equations are determined by linear transformation of Cauchy stress tensor (σ) as below.

$$\tilde{S}' = L' : \sigma \text{ and } \tilde{S}'' = L'' : \sigma \tag{2.3}$$

The generalized form of the above equations is shown below.

$$X_i = |\alpha_1 b_{1i} - \alpha_2 b_{2i}|^a + |\alpha_3 b_{1i} + 2\alpha_4 b_{2i}|^a + |2\alpha_5 b_{1i} + \alpha_6 b_{2i}|^a - 2(\bar{\sigma}/\sigma_i)^a = 0 \tag{2.4}$$

where, i denotes different loading states along directions, respectively [46].

There are a large number of material models located on LS-Dyna software. The material model *MAT_BARLAT_YLD200 has been employed in this thesis study to simulate the mechanical behavior of the C-PHE forming process by considering its effectiveness in demonstrating the anisotropic behavior of rolled sheet metals and more than 5 years of serial experience of Home Comfort in Manisa, Türkiye.

2.4.2 Mesh Sensitivity Analysis

Mesh sensitivity analysis was carried out to evaluate the effect of different simulation variables on numerical stability [47]. The preprocessor of HYPERMESH software has been employed to create nonuniform mesh sizes varying from 0.5 to 2 mm to analyze mesh discretization sensitivity. A series of analyses are carried out using the six different mesh patterns for the die, the blank, the blank-holder, and the punch with the finer mesh to prove sensitivity. The size of the mesh elements, number of mesh, minimum and maximum shell thickness on blank have been listed, as shown in Table 2.3.

Table 2.3. Mesh data for the discrete model of the C-PHE on LS-Dyna

Element Size (mm)	**<#> of Mesh**	**Min. Shell Thickness (mm)**	**Max. Shell Thickness (mm)**
0.5	203156	0.23	0.3473
0.75	168706	0.211	0.3688
1	155819	0.2094	0.3731
1.25	150072	0.2473	0.3486
1.5	146843	0.2464	0.3462
2	143759	0.2428	0.3774
	AVERAGE	0.23115	0.360233333
	STD. Deviation	0.015861457	0.01312233
	STD. Dev. / Average	7%	4%

The minimum shell thickness value is taken as a more critical value by considering Bosch HC norms and standards about C-PHE production. The minimum thickness limit of SS plate is given as 0.20 mm in Bosch HC material order specification of C-PHE production to minimize production and field failure caused by exposed cyclic pressure and thermal loads.

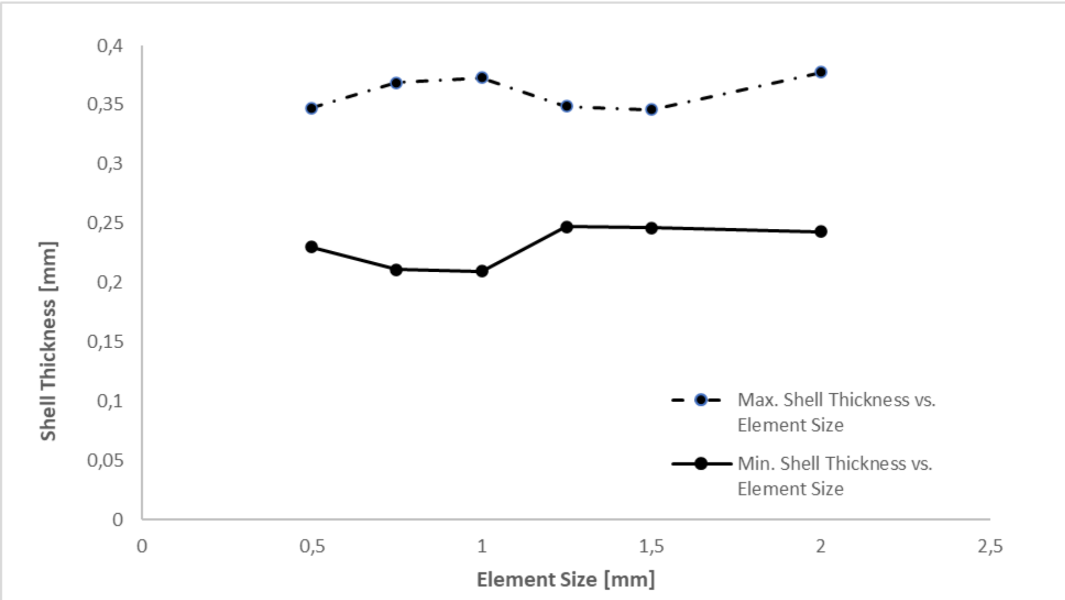

Figure 2.9. Representation of the mesh sensitivity analysis

Thickness reduction is observed more clearly by employing 0.75 mm and 1 mm sized elements in FEA simulations as shown in Figure 2.9. As a result, 1 mm sized fine elements are selected while conducting FEA simulations in this thesis by considering the high probability of deteriorating the aspect ratio of elements and minimization of computational time. Meshed forming elements of the C-PHE are represented in Figure 2.10.

Figure 2.10. The meshed forming elements of the C-PHE.

2.4.3 Numerical Setup

The FEA simulations were carried out with FEA software LS-Dyna version 4.8.29. SMF process of C-PHE with alternative raw materials was modeled separately. The complexity of the pattern of C-PHE was taken into consideration to mimic the production process. Due to this reason, symmetry models were not employed to reduce computational time. All the tools used in the simulation were modeled as rigid body elements except for the lower die. The lower die was modeled as a stationary tool. Contact type between blank holder, blank, and punch was selected as *CONTACT_AUTOMATIC_SURFACE_TO_SURFACE and *FORMING_SURFACE_TO_SURFACE by considering thickness offsets and irregular shape of formed surface as shown in Figure 2.11 and Figure 2.12 accordingly.

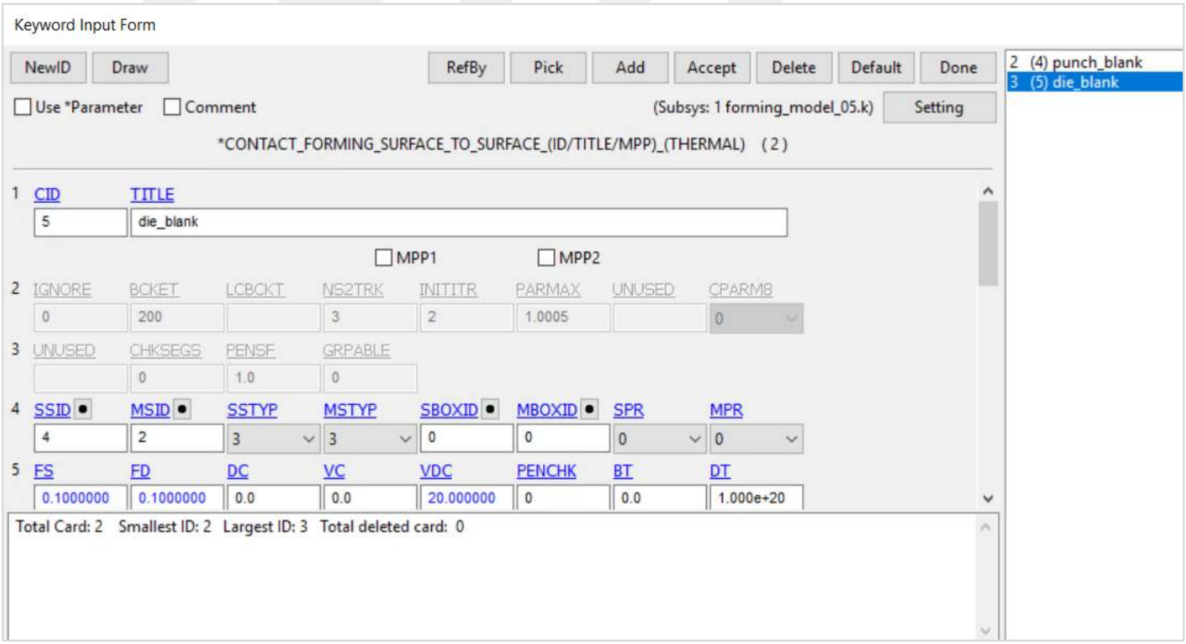

Figure 2.11. The contact type modeling between the die & the blank on LS Dyna.

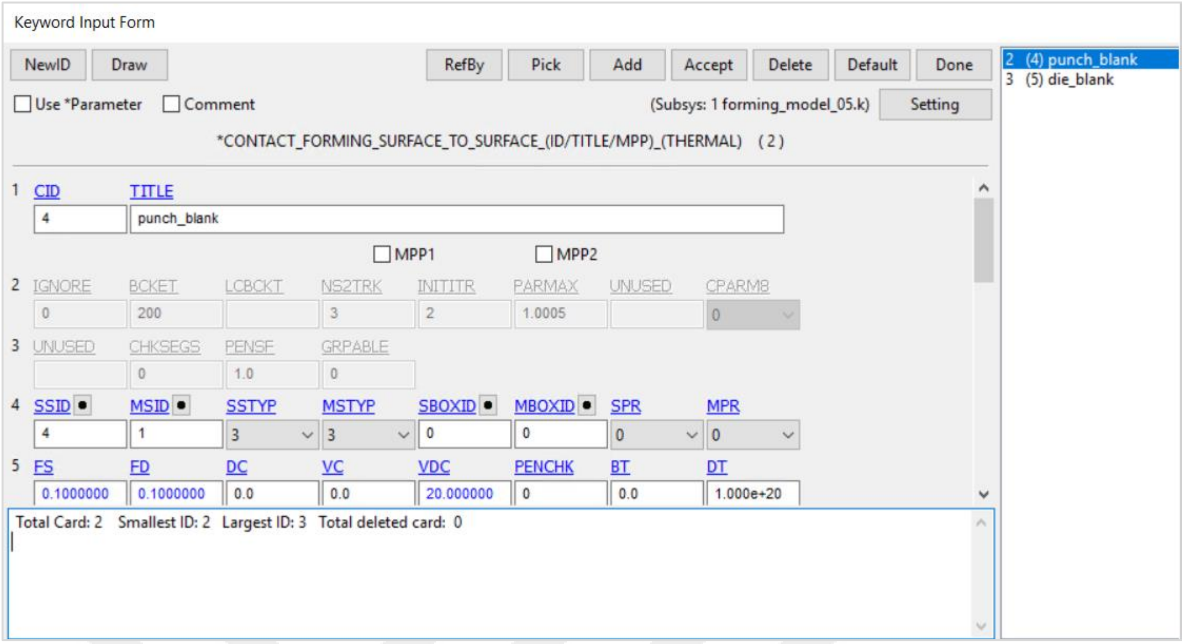

Figure 2.12. The contact type modeling between the punch & the blank on LS Dyna.

The YLD2000 yield function implemented as *MAT_BARLAT_YLD2000 in LS Dyna was used for modeling the anisotropic behavior of blank for 316L SS and 304L SS materials. The material cards for 316L SS and 304L SS are represented in Figure 2.13 and Figure 2.14 respectively.

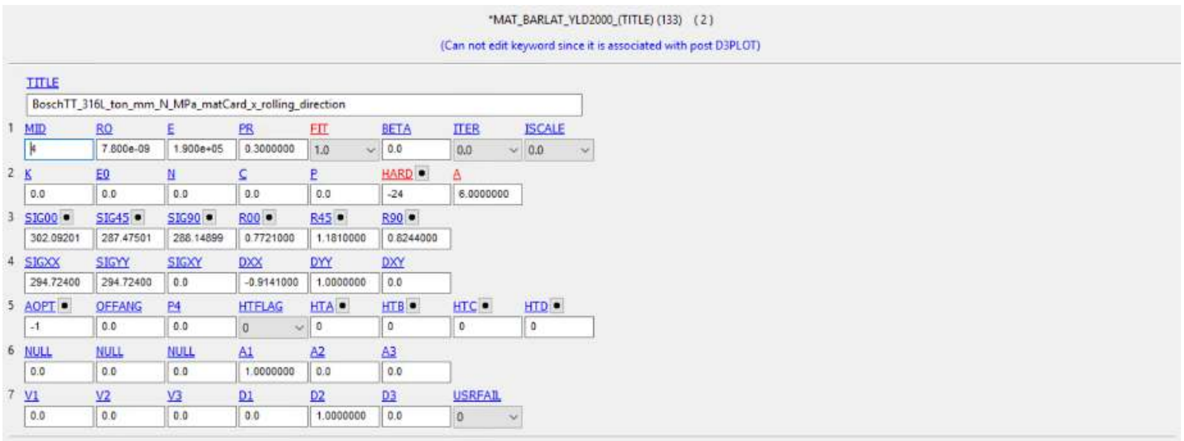

*Figure 2.13. The *MAT_Barlat_YLD2000 material card for the 316L SS.*

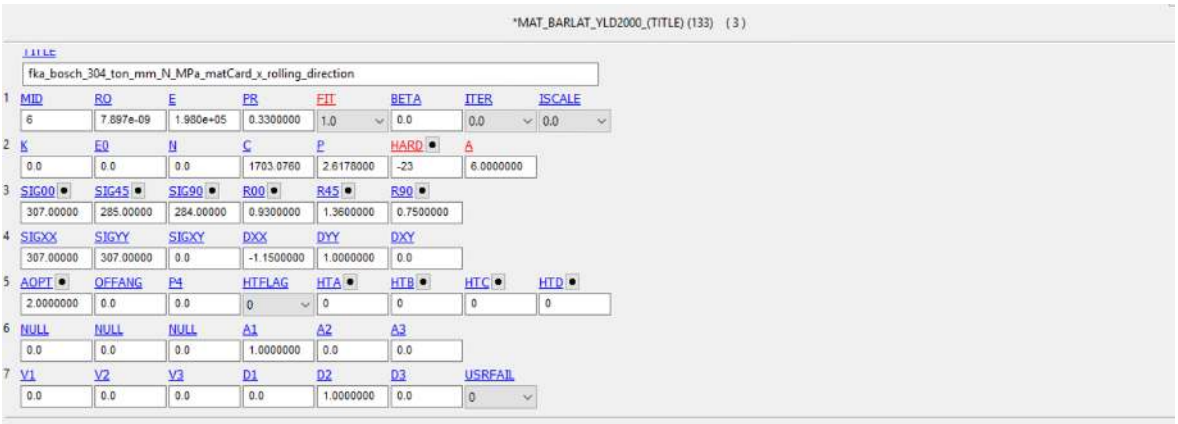

*Figure 2.14. The *MAT_Barlat_YLD2000 material card for the 304L SS.*

The punch was moved with a specific load and displacement curve applied in Bosch Home Comfort C-PHE production in Manisa Plant as illustrated in Figure 2.15 and Figure 2.16.

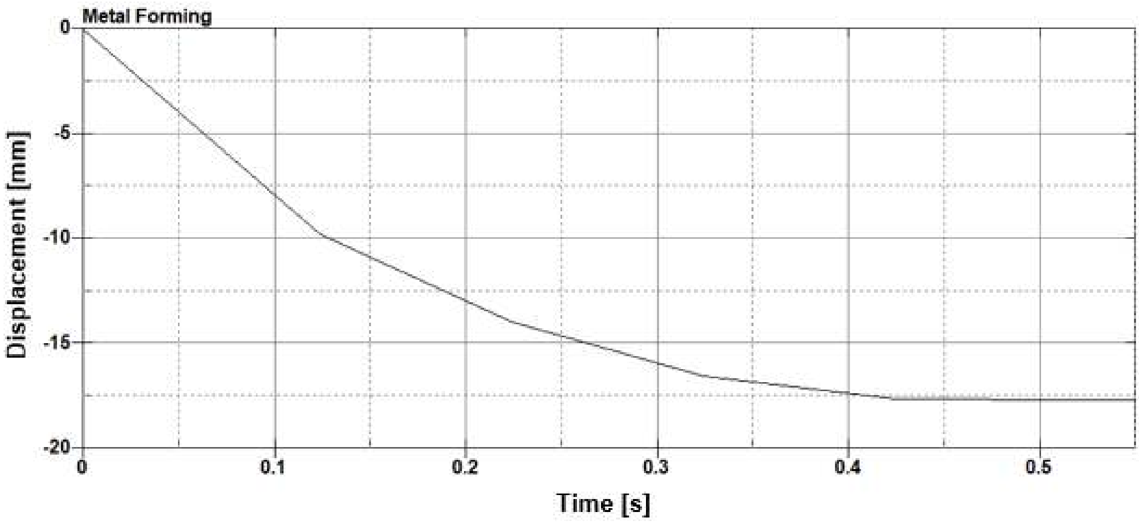

Figure 2.15. The punch displacement with respect to time implemented in FEA simulation on LS Dyna.

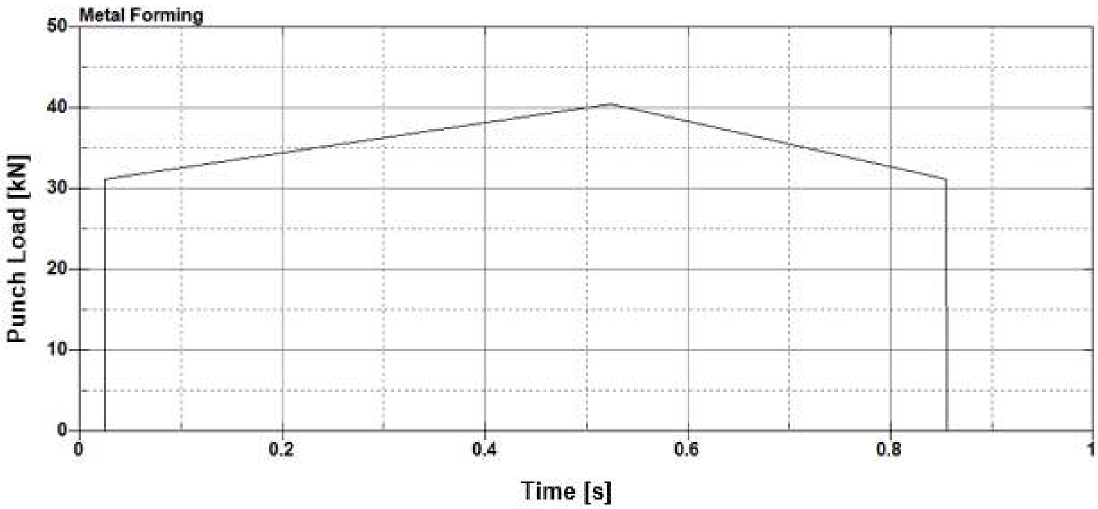

Figure 2.16. The punch load with respect to time implemented in FEA simulation on LS Dyna.

2.4.4 FEA Results

The thickness, the raw material, and strain rate of the fine blank have a great influence upon the shape of the workpiece. For a comprehensive approach of design and process parameters' effect on the form of the workpiece, achieved by FEA simulations, have been plotted in Figure 2.17, Figure 2.18, and Figure 2.19, respectively.

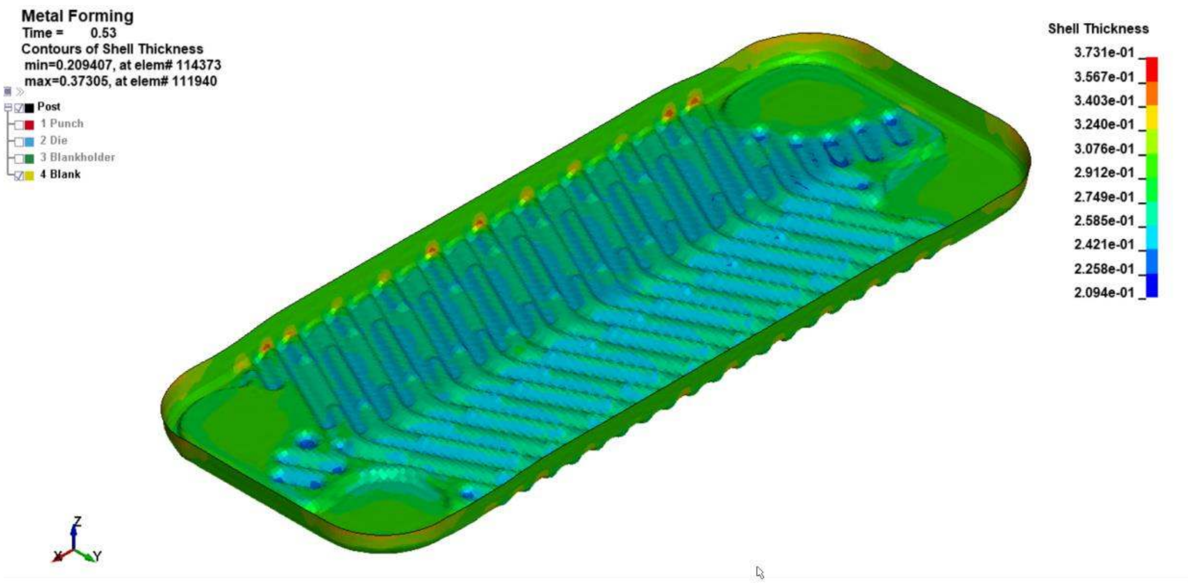

Figure 2.17. Shell thickness of the 0.3 mm thick 316L SS blank.

For the measuring impact of raw material, 0.3 mm thick 316L SS and 304L SS made blanks have been designed. After conducting FEA simulation for two workpieces, the thickness reduction of 316L SS blank was bigger relative to 304L made under the same production process loads. The FEA simulations showed that the raw material characteristics have a great impact on the thickness distribution so the response of workpieces with different raw materials were illustrated in Figure 2.18.

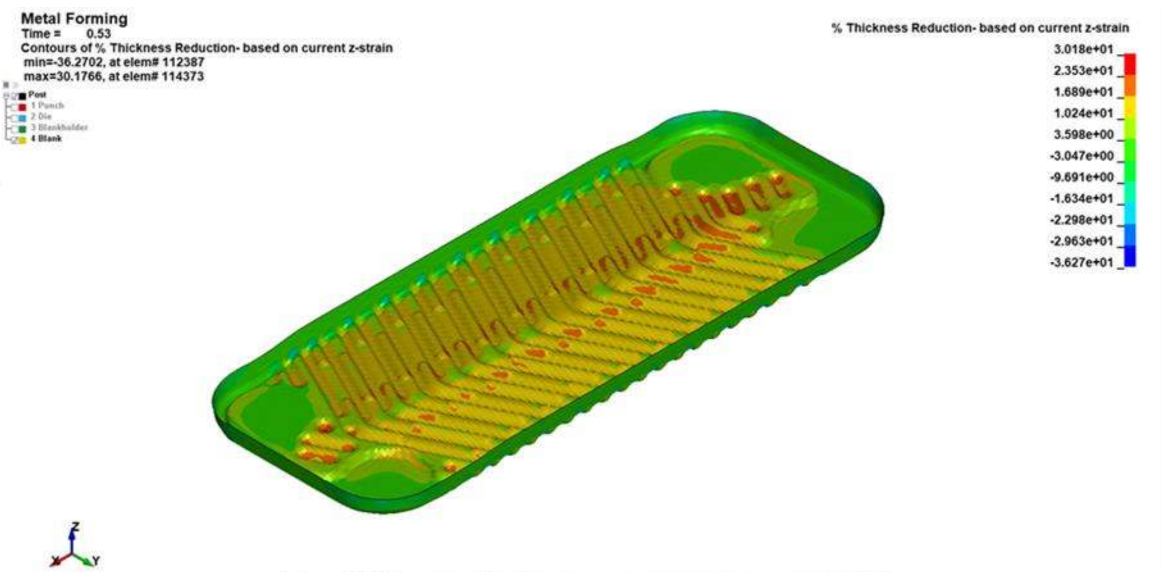

(a) Thickness reduction percentage for 0.3 mm 316L SS

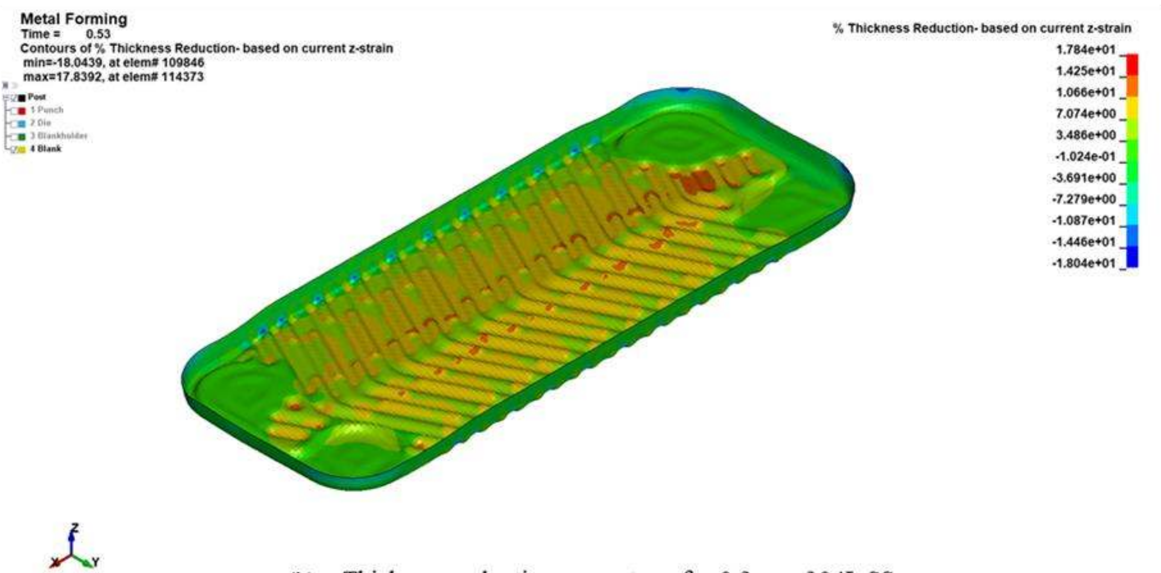

(b) Thickness reduction percentage for 0.3 mm 304L SS

Figure 2.18. Thickness reduction distribution for the 0.3 mm blanks of (a) the 316L SS, and (b) the 304L SS.

To measure influence of raw material on plate thinning, 0.8 mm thick 316L SS and 304L SS made blanks have been designed. After performing FEA simulations, the thickness reduction of 316L SS blank was bigger relative to 304L made under same production process loads. The FEA calculations showed that the blank thickness has great impact on the thickness distribution so that the response of workpieces with different raw materials. It can be seen that the impact of blank raw materials decreases while increasing the blank thickness as illustrated in Figure 2.19.

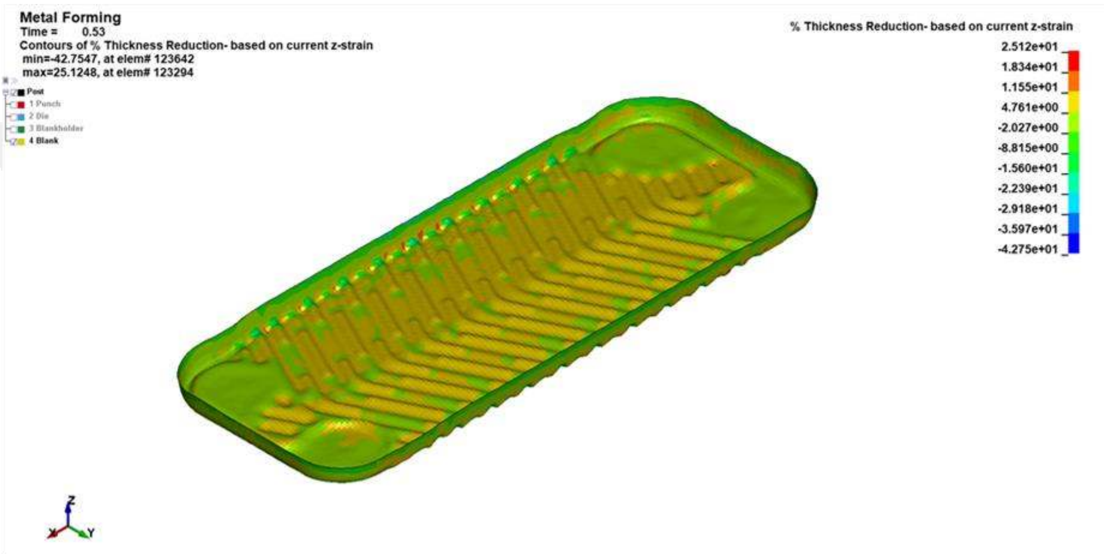

(a) Thickness reduction percentage for 0.8 mm 316L SS

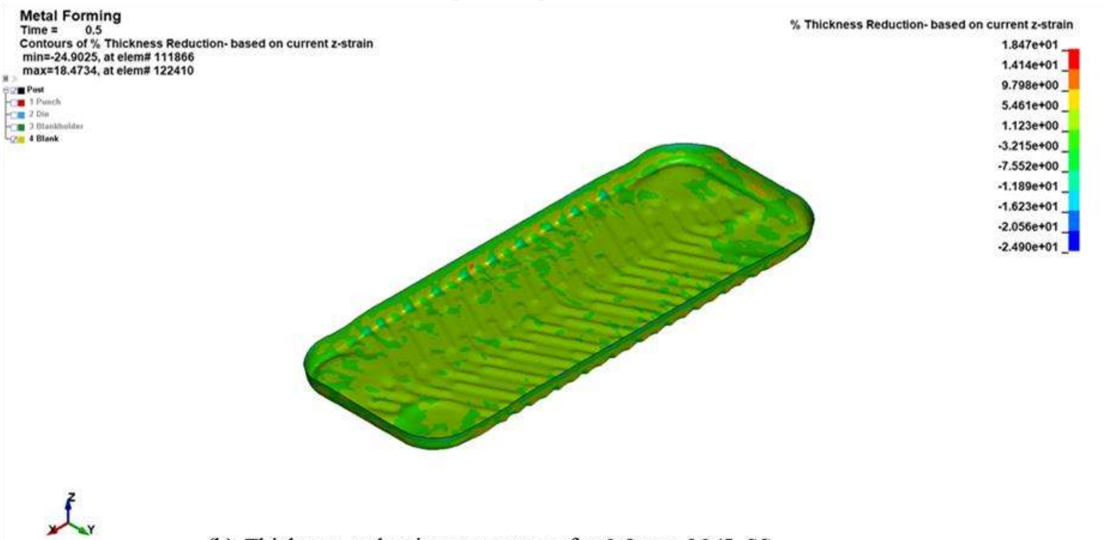

(b) Thickness reduction percentage for 0.8 mm 304L SS

Figure 2.19. Thickness reduction distribution of 0.8 mm blank made of (a) the 316L SS, and (b) the 304L SS.

The main objective of changing the strain rate during forming simulations is measuring the influence of the process parameter on the workpiece. The process parameters can shorten the production time of C-PHE. However, it is experienced in C-PHE production that process parameters have bigger impact of the quality of final workpiece. During the product lifecycle of C-PHE, there are several loads exposed to plates such as temperature, cyclic pressure, and mechanical forces. It is seen that lowering strain rate leads to lower thickness reduction for the same workpiece as shown in Figure 2.20. Hence, strain rate should be taken into consideration during optimization process to obtain robust C-PHEs with cost advantage.

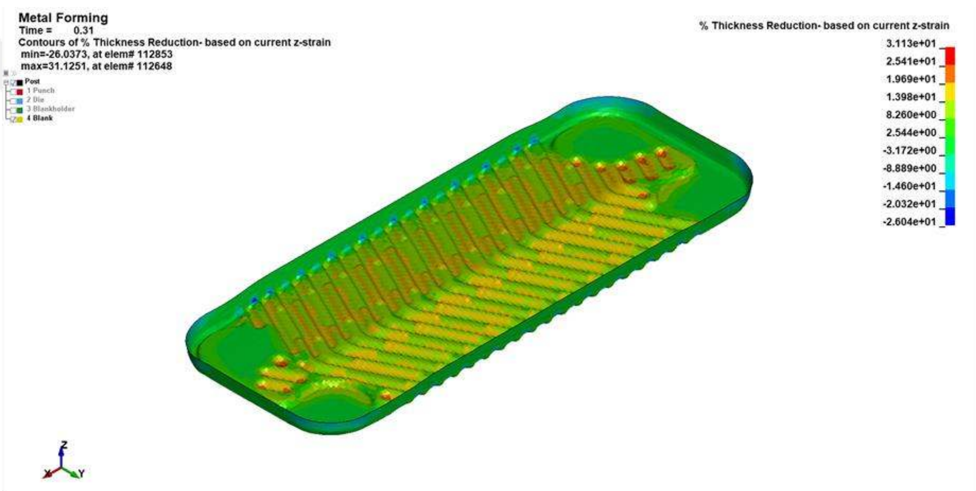

Thickness reduction percentage for 0.5 mm 316L SS by scaling strain rate with 0.6.

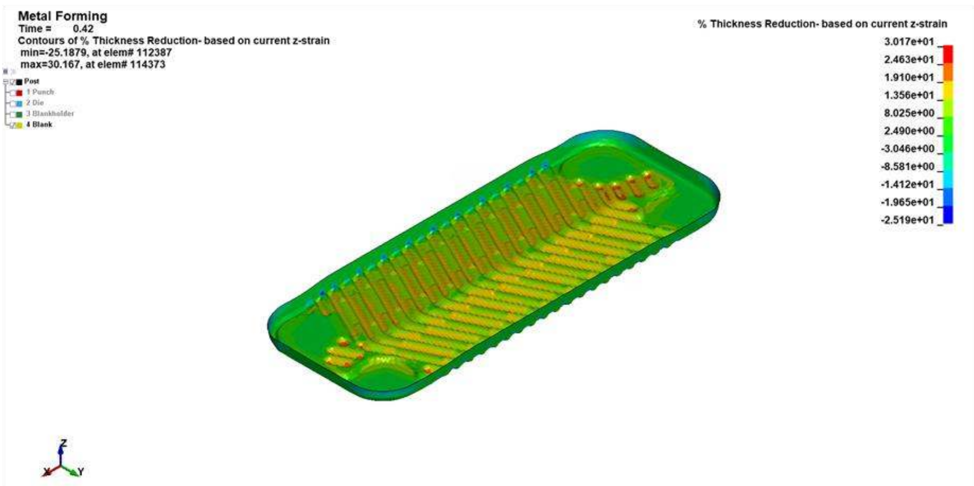

Thickness reduction percentage for 0.5 mm 316L SS by scaling strain rate with 0.8.

Figure 2.20. The thickness reduction distribution of blank made of 316L SS according to the different strain rates.

Chapter 3:
Machine Learning Model

3.1 Calculation Procedure

This section starts by outlining the calculating techniques that were employed for this investigation. Then, a brief description of the used ML models is given, followed by a comparison of the models' skills. Finally, the sample issues that were used to illustrate and discuss influences on model correctness are.

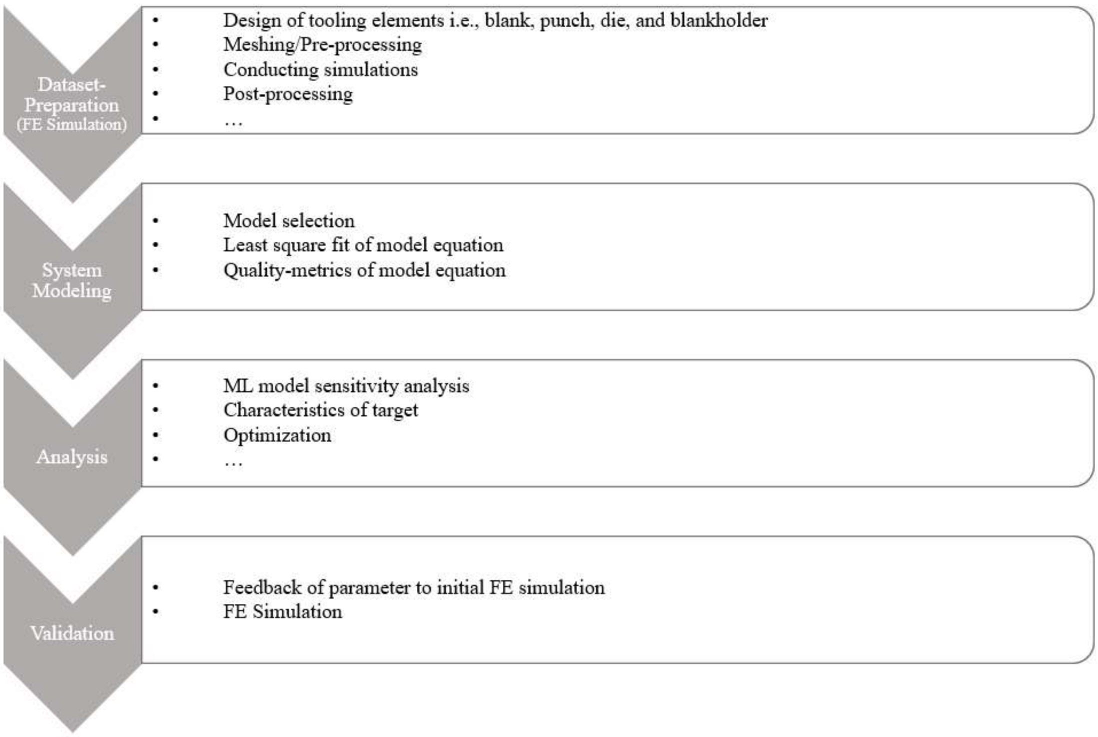

Figure 3.1. Schematic sketch of the calculation procedure of this thesis, similar to [48].

The calculation procedure utilized in this study is parallel to the procedure depicted in [48]. The fundamental concept is to construct a simplified model using data from FEA simulations. This model is then used for forecasting system characteristics and design optimization.

The calculation procedure is split into four steps as below.

1. Dataset-preparation,
2. System modeling

3. Analysis
4. Model validation

which are represented in Figure 3.1.

3.2 Dataset Preparation

In SMF, a common processing trends in automotive and HVACR industries is observed such reducing raw material weight and optimizing performance [49]. However, the low weight raw material usage has led to some mechanical deformations such as necking and wrinkling which causes excessive thickening [30], [50]. The failure of excessive thinning is caused while the dominant stress on plate surface is in tensile mode [51]. Since excessive thinning and its characteristics mainly depend on a number of design and process parameters, a quantitative approach of excessive thinning by FEA is generally possible in restricted cases. In Bosch Home Comfort, a detailed description of excessive thinning of the plates requires visual inspection. In order to eliminate manual inspection and trial-error solution and to activate a reasonable explanation for excessive thinning based on cases, an intelligent analysis of the available data is crucial.

An existing FEA-model's material parameters were updated through model optimization to better mimic the C-PHE production process [52]. However, getting closer to the production process is also not adequate looking at a series of products. Tolerances required for manufacturing inevitably result in variances in the final geometry. Distinctive properties of the various product are produced as a result of these variances. They are not decisive; therefore, the consequent scatter is also ambiguous.

In this thesis, the C-PHE production process combination was considered in FE analysis. The C-PHE production process combination is demonstrated in Figure 2.5. The three-dimensional FEA model was built to perform simulation analysis on LS-Dyna for the C-PHE production process combination. The Barlat material card and simulation parameters have been proven to predict C-PHE production process according to Bosch Home Comfort internal standards. The input and output data for ML model were collected based on FEA simulation on LS-Dyna to investigate the impact of input parameters on outputs on the SMF thinning. Certain input parameters are allowed to be modified except for the plate pattern since the plate pattern of C-PHE is protected by patent. The patent can be affected by modifying the pattern. Moreover, it may cause conflict with other

Intellectual Properties. Hence, input parameters used in ML analysis are limited to the raw material types, geometrical and process parameters. To illustrate deviation on local plate thinning based on variation of input parameters, certain mesh elements were selected, and plate length was normalized according to the table below.

Table 3. 1. ID of mesh element and the normalized distance used in forming simulation on LS-Dyna.

ID OF MESH ELEMENT	Normalized Distance
A113963	0
U114504	0,1
AO115253	0,2
BI115747	0,3
CC116456	0,4
CW117233	0,5
DQ117091	0,6
EK117797	0,7
FE118727	0,8
FY120172	0,9
GS119634	1

The impact of these input parameters on sheet metal thickness according to the normalized plate length is demonstrated in Figure 3.2. In this graph, the input parameters were selected as 0.3 mm thick 316L SS, 0.3 mm thick 304L SS, 0.3 mm thick 304L SS with a 0.6 strain rate scaling ratio, and 0.3 mm thick 304L SS with a 0.6 strain rate scaling ratio. After performing simulation, the thickness reduction values for all mesh elements on LS-Dyna simulation and adopted to the abovementioned certain path through formed plate of C-PHE to gathering deviation of plate thickness on same mesh element for observing the influence of input parameters on thinning. After results of FEA simulations, it is observed that the different raw materials usage for C-PHE production has significant effect on thickness reduction at entrance area where the ports are located.

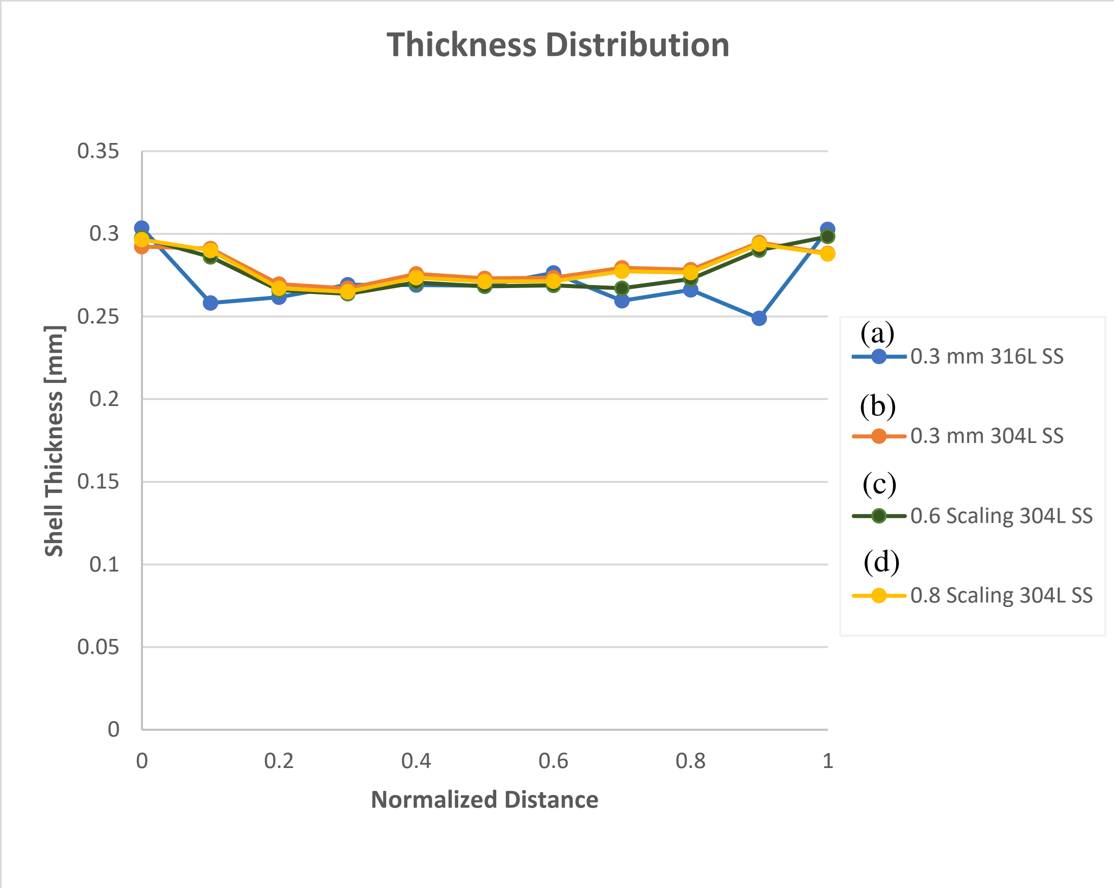

Figure 3.2. The thickness distribution throughout plate for a certain path for the cases;(a) the 0.3 mm thick 316L SS, (b) the 0.3 mm thick 304L SS, (c) the 0.3 mm thick 304L SS with 0.6 scaling ratio, and (d) the 0.3 mm thick 304L SS with 0.8 scaling ratio.

By considering the influence of input parameters on plate thinning, the dataset was prepared based on FEA simulation inputs and outputs. In thesis dataset, there are 66 sets of data placed by covering the alternative plate raw materials, the process variations, and the design parameter variations. The dataset can be reached in Table 0.1.

3.3 System Modeling

Regardless of the model's capacity for prediction, dataset preparation is one of the crucial components of design optimization by employing ML model since each piece of data the model interprets by utilizing a suitable dataset. Therefore, selecting the relevant qualities to collect and separating relevant from redundant information are crucial for a successful ML model deployment. As a result, before gathering the data that were specifically indicated in the preceding part, the aspects that have an impact on design optimization of C-PHE were thoroughly searched for in this work.

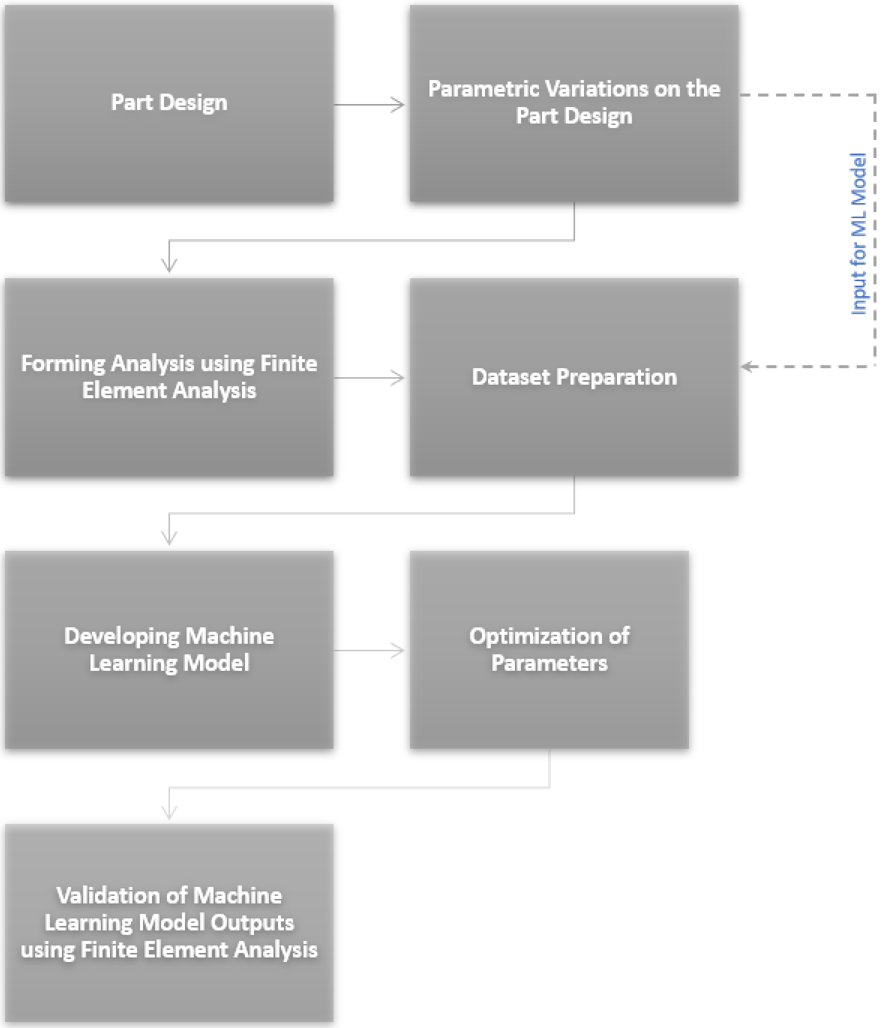

Figure 3.3. Diagram of the developed ML model.

A sophisticated literature review has been made based on the aforementioned constraints to develop an appropriate machine learning model for design optimization of C-PHE [48]– [82]. It has been noticed that there are frequent usages of specific models such as regression models and ANNs with different algorithms have taken place for SMF applications while performing literature review. As represented in Figure 3.3, developing ML model for this work is also one of the crucial parts of this study. During ML model development phase, regression models located on MATLAB regression learner module were employed. While design parameters were selected as the input parameters, the thinning percentage was selected as the target value. Bagged Trees regression model has the best prediction accuracy with minimum root mean squared error (RMSE) value as 4.7882. The prediction of the Bagged Trees model is shown in the graph below.

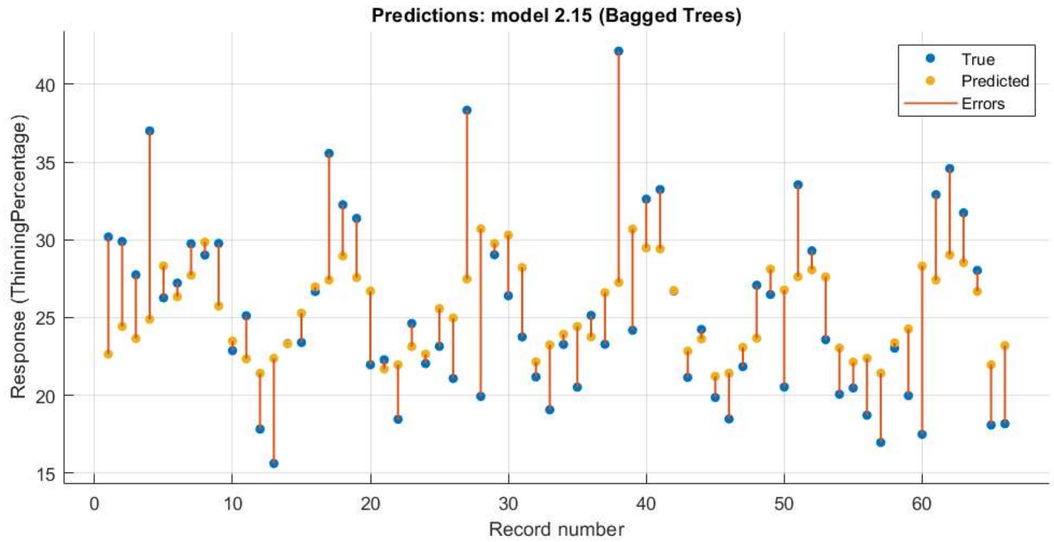

Figure 3.4. Prediction-Error graph of the bagged trees.

In order to achieve the model having lower RMSE value, ANN models with different algorithms had been employed. While model selection for best prediction in this work, the default adjustments were used for three different algorithms as mentioned in below table.

Table 3.1. The default parameters for ANN models on MATLAB.

Algorithm	Number of Layer	Training Data [%]	Test Data [%]	Validation Data [%]
Levenberg-Marquardt	10	70	15	15
Bayesian Regularization	10	70	15	15
Scaled Conjugate Gradient	10	70	15	15

The capability of regression and neural network models based on prediction accuracies have been listed in Table 0.2 after training regression models and ANN models. According to the graph below, the best prediction accuracy was obtained by employing ANN models.

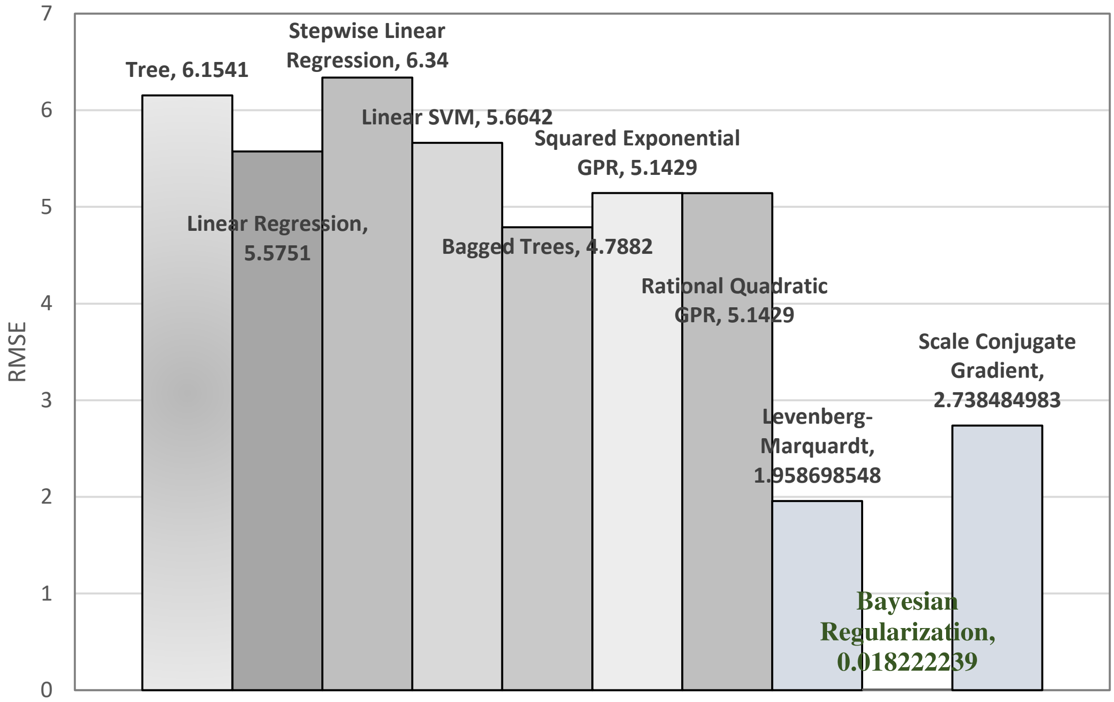

Figure 3.5. Comparison of the ML models based on prediction capabilities.

The R values of each ANN models that are Levenberg-Marquardt (LM), Bayesian regularization, and Scale Conjugate Gradient, respectively were obtained with using the abovementioned default parameters. The best prediction accuracy with the default parameters was obtained by utilizing the Bayesian Regularization algorithm based on R value comparison. The R values of established model with different algorithms are represented in Figure 3.6, Figure 3.7, and Figure 3.8 individually.

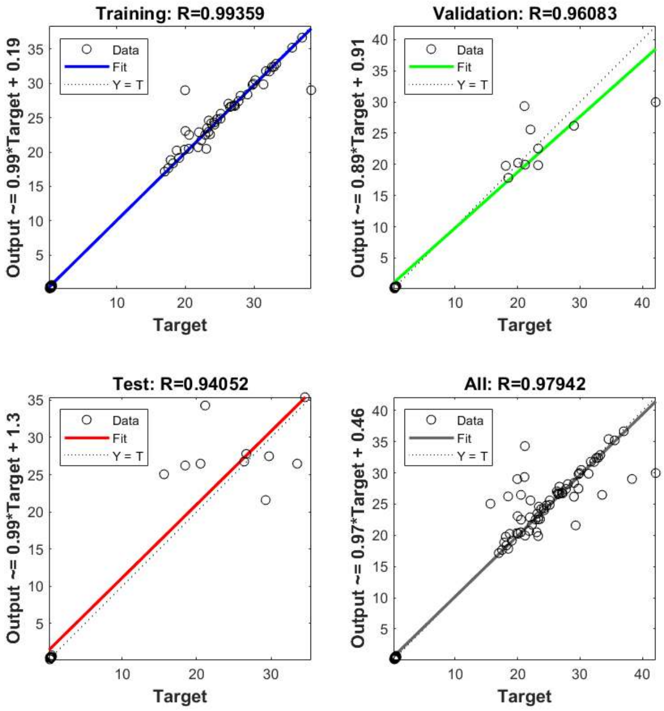

Figure 3.6. The prediction performance of Levenberg-Marquardt algorithm.

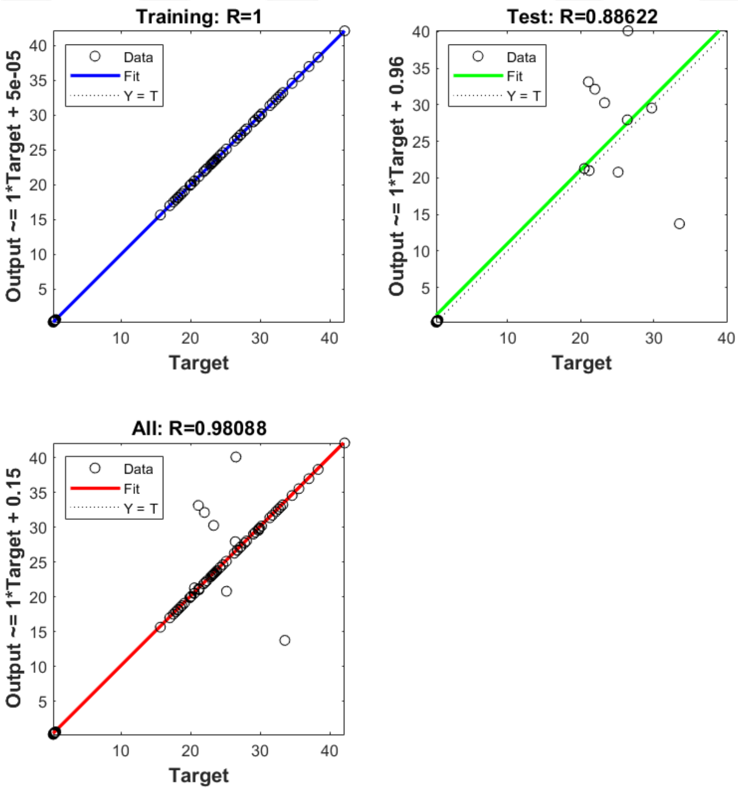

Figure 3.7 The prediction performance of Bayesian Regularization algorithm.

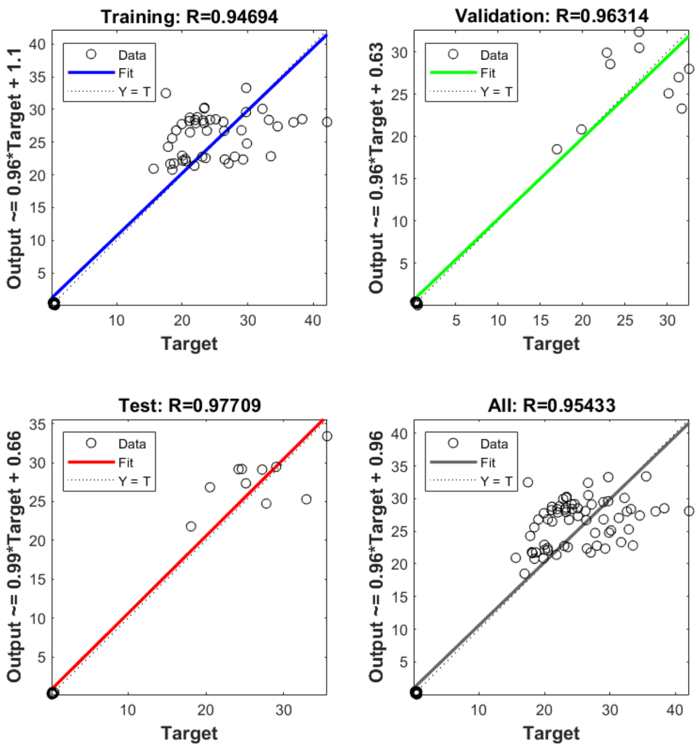

Figure 3.8 The prediction performance of Scale Conjugate algorithm.

3.4 ML Model Optimization

The optimization process of ANN model is to find out the relation that will drive ML model outputs as close as desired values. In order to solve this problem, optimization is required for this study. It was observed that data separation while training the ML model has an impact on the quality of results. The mean square error, MSE, is defined as

$$MSE = \frac{1}{N} * \sum(y - \hat{y})^2 \qquad (3.1)$$

where, N is number of data points, y is the real output, $\hat{y}$ is the predicted value. To optimize prediction accuracy, MSE values of the ANN model with different data separation are calculated with the above equation. In this study, it was observed that separating the dataset into training, test, and validation data as 70%, 15% and 15% gave the minimum MSE as 0.0004.

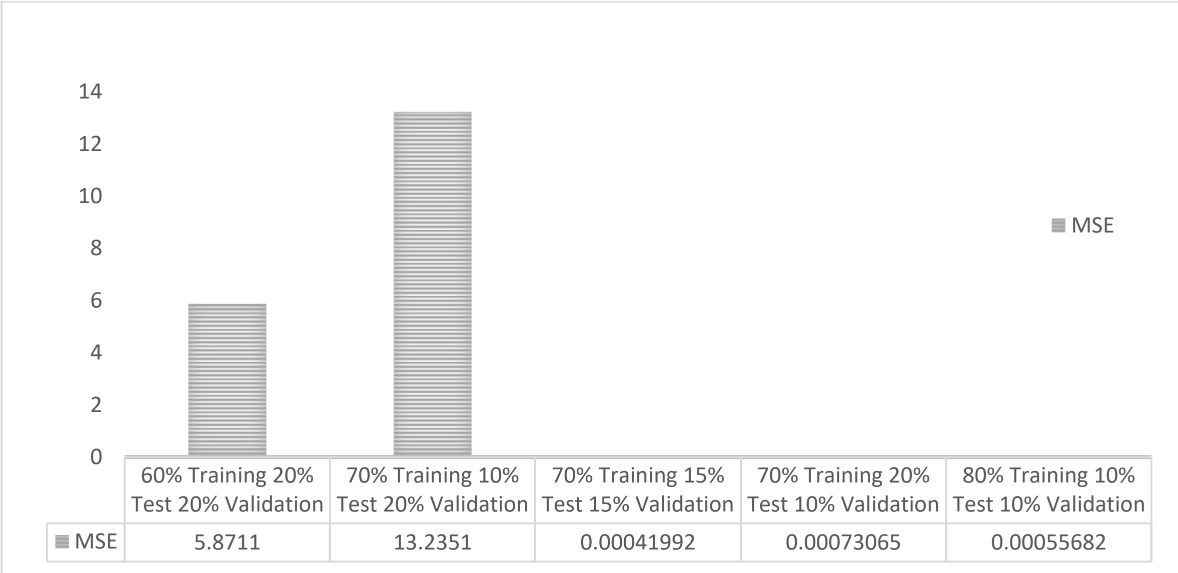

Figure 3.9. The performance of the ANN model with Bayesian Regularization algorithm with different data separation.

Regardless of the ANN model's structure, there are two common physical components, the processors called neurons and the connection between neurons. Information can be processed by neurons in a variety of ways, and there are numerous ways to link neurons. A variety of neural network structures can be formed by utilizing various processing components and by connecting them in various ways. Consequently, neuron structure in the ANN model can influence the prediction accuracy. During the testing phase of the current ANN model, a trial-and-error method was employed to find out the number of neurons, as it currently also represents the common approach in practice. Therefore, the neuron sensitivity analysis was performed to improve the prediction accuracy of the ANN model. To achieve this, different ANN model configurations were created for training. To compare the impact of neuron numbers, the ANN model was run with different numbers of neurons as shown in Figure 3.10.

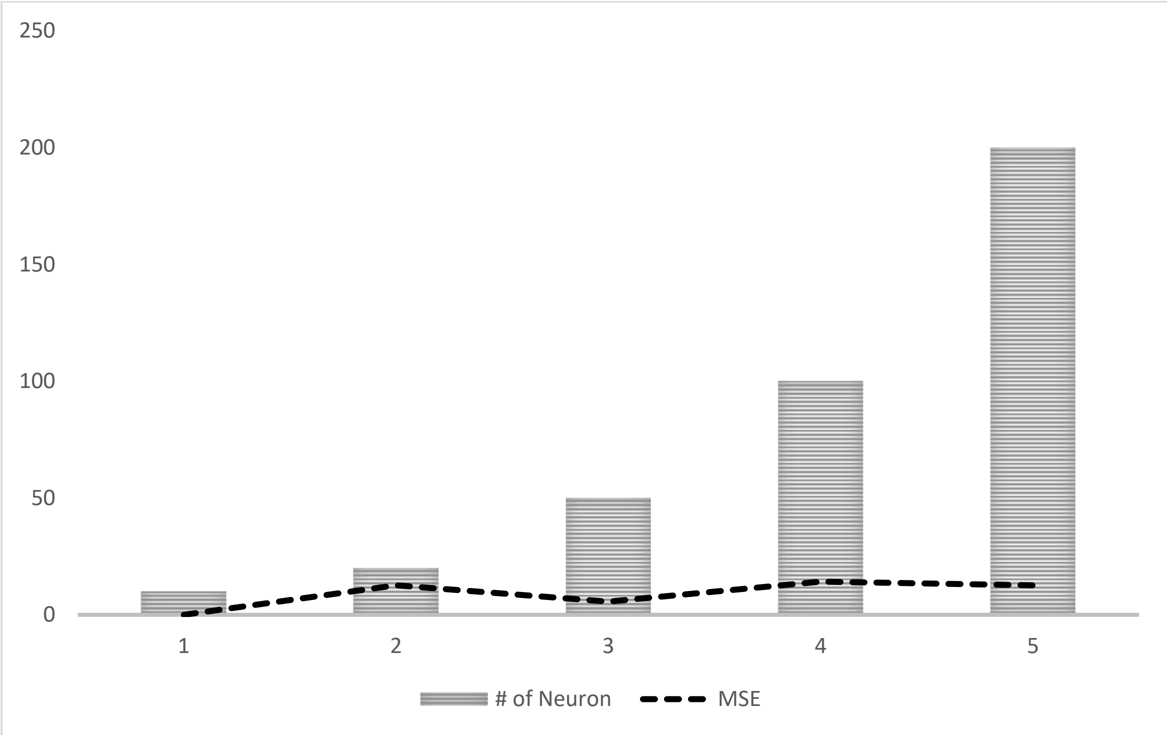

Figure 3.10 The neural sensitivity analysis of the ANN model.

Based on the results shared in the above figure, the best prediction accuracy was obtained with 50 neurons. Thus, the architecture of the developed feedforward network in the chosen configurations is exemplified in Figure 3.11.

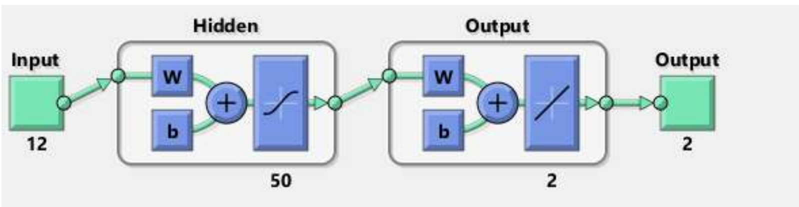

Figure 3.11. Architecture of the optimized ANN model

3.5 *ML Model Results*

The experiment has been conducted on a computer with quad-core Intel i7-10850H CPU 2.7 GHz processor and 32 GB memory. It was equipped with Intel® UHD Graphics GPU and 16 GB memory.

The neural network architecture was established in the above section requires training to enable an appropriate design characteristic of C-PHE generation. Here, the qualified prediction data set is necessary and must be generated. While generating prediction data set, the design of experiment (DOE) technique was employed. In order to perform the DOE, Design Expert v6.0.8 software was used. While building the input data set on Design Expert, D-Optimal Design method was used as shown in Figure 3.12. The response and factors of the DOE was determined as essential to this work. Consequently, there are 507 cases generated from the DOE approach as the input data set by covering all spectrums of components.

Figure 3.12. The D-Optimal user interface of Design Expert Software for DOE.

The generated input file was imported to workspace on MATLAB. Then, the trained ANN model was run with the input file to generate prediction results of the different design and process parameters. The prediction accuracy of the ANN model was determined based on R value. R value is calculated as below.

$$R^2(y,\hat{y}) = 1 - \frac{\sum_{i=1}^{l}(y_i - \hat{y}_i)^2}{\sum_{i=1}^{l}(y_i - \bar{y}_i)^2} \tag{3.2}$$

where y is the real value, and $\hat{y}$ is the predicted value. After the second run of the ANN model, the performance results of the prediction were obtained as R=0.98332 which indicates good correlation between real value and prediction as shown in Figure 3.13. As mentioned earlier, accurate and precise results can be obtained from the trained model when the R value closes to 1. Thus, the outputs of the second run were used for the design optimization of C-PHE.

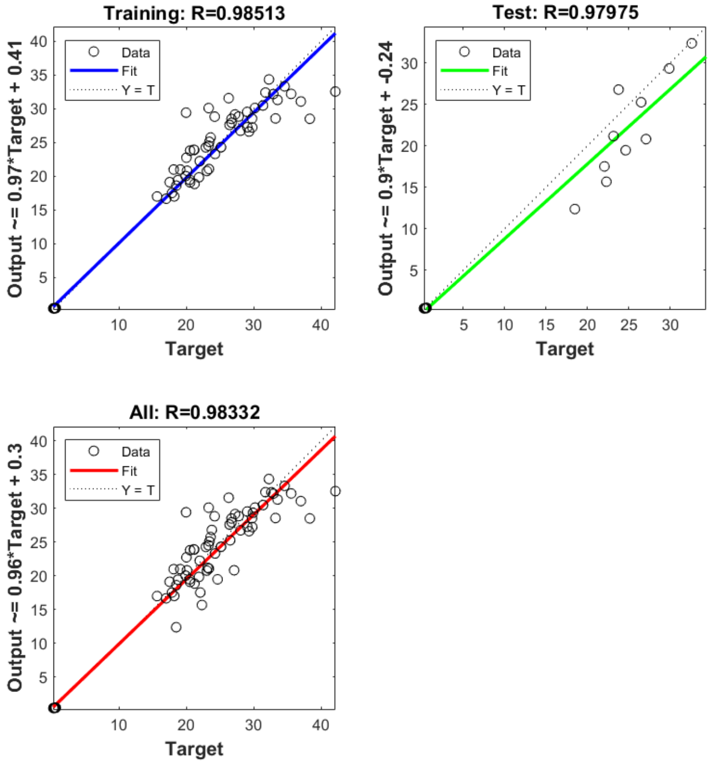

Figure 3.13. The R value of the ANN model.

The best training performance of the developed ANN model was obtained at epoch 87 as 5.1338. The training and test performance of the ANN model was illustrated in Figure 3.14. According to Figure 3.14, the trend of training and test performance after epoch 87 follows parallel path and is consistent.

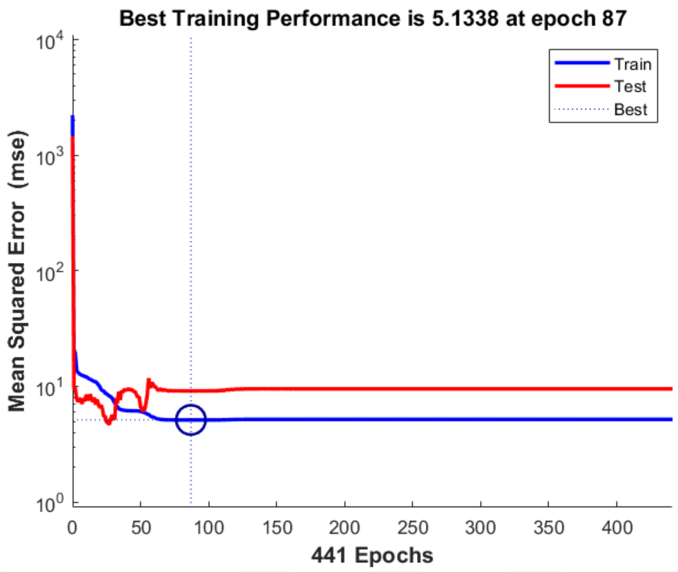

Figure 3.14. Performance of the developed ANN model.

The histogram which illustrates the zero-error instance is shown in Figure 3.15

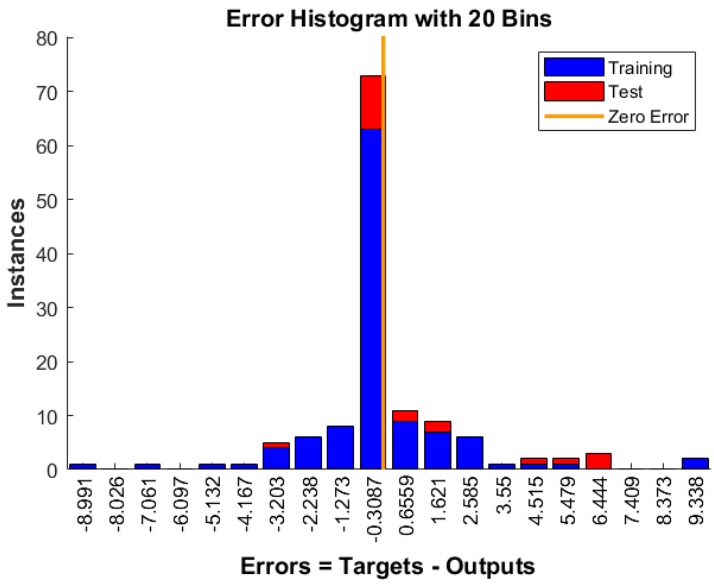

Figure 3.15. Error histogram of the ANN model

As an outcome of the ANN model, the design and process parameters were determined according to Bosch Home Comfort standards as minimum 20 mm plate thickness as represented in Table 3.2.

Table 3.2. The predicted design and process parameters

	Cr	Ni	Mo	C	Mn	P	S	Si	N	Sheet Thickness [mm]	Strain Rate	Max Effective Surface Stress [Mpa]	Thinning Ratio [%]	Minimum Thickness [mm]
(a)	16	10	2	0.03	2	0.045	0.03	0.75	0.1	0.25	0.8	1500	19.783	0.201
(b)	17.5	8	0	0.03	2	0.045	0.015	1	0.1	0.3	1.4	2250	32.847	0.201
(c)	16	10	2	0.03	2	0.045	0.03	0.75	0.1	0.35	1.4	2250	40.583	0.208
(d)	16	10	2	0.03	2	0.045	0.03	0.75	0.1	0.25	0.9	2000	15.697	0.211
(e)	16	10	2	0.03	2	0.045	0.03	0.75	0.1	0.25	1.1	1250	15.452	0.211
(f)	16	10	2	0.03	2	0.045	0.03	0.75	0.1	0.3	0.5	2000	26.789	0.220

3.6 *ML Model Validation*

The Bayesian Regularization algorithm was utilized in the ANN model to solve this optimization problem. The intricate approach is based on the creation and upkeep of a pattern of search points and uses the training and test data as a point of projection desired trend in order to identify outputs of the dataset prepared by performing DOE analysis. By inspecting Figure 3.13, the neural network containing hidden layer with 50 neurons was selected optimum model.

The real output and the optimum (50 hidden neurons) ANN model approximated output are shown in Table 3.2. In order to validate results, the FEA analysis was performed for the cases shared in Table 3.2. The consequences of the FEA simulation performed on LS-Dyna software are illustrated in Figure 3.14.

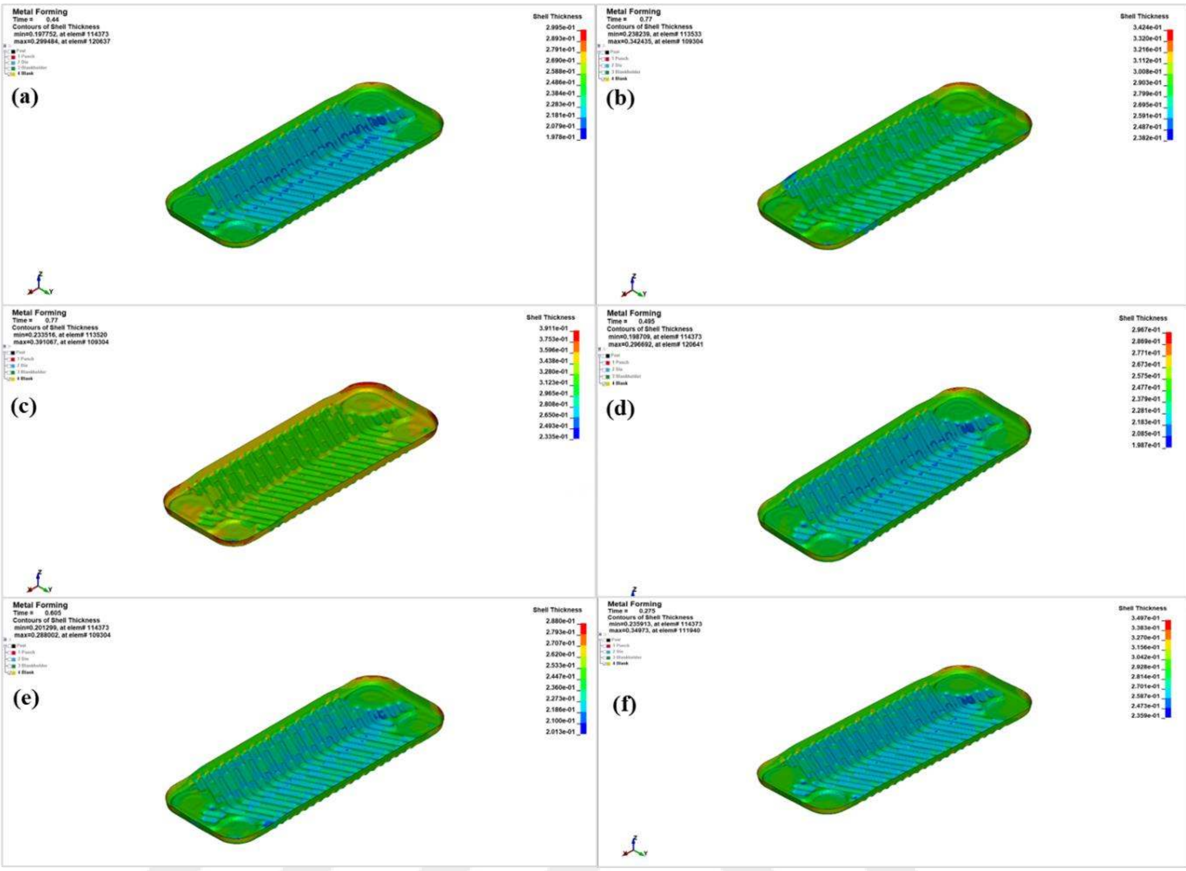

Figure 3.16 The outputs of the FEA simulation under the cases given in Table 6; (a) the 0.25 mm thick 316L SS with 0.8 strain rate scaling, (b) the 0.3 mm thick 304L SS with 1.4 strain rate scaling, (c) the 0.35 mm thick 316L SS with 1.4 strain rate scaling, (d) the 0.25 mm thick 316L SS with 0.9 strain rate scaling, (e) the 0.25 mm thick 316L SS with 1.1 strain rate scaling, (f) the 0.35 mm thick 316L SS with 0.5 strain rate scaling.

The proposed ANN model with Bayesian Regularization algorithm was compared with the FEA simulation results that were performed on LS-Dyna software by using the dataset listed in Table 3.2. The dataset was fed directly to the LS-Dyna software to conduct FEA simulation. Notably, the optimized ANN model achieved good performance. The comparison between the ANN model and FEA simulation outputs were shared in Table 3.3.

Table 3.3. The comparison of the minimum thickness of the sheet metal after forming process between the ANN model and the FEA simulation.

Minimum thickness of the sheet metal after the forming process			
Cases	The ANN Model Output [mm]	The FEA Simulation Output [mm]	Error [%]
(a)	0.201	0.1978	1.59
(b)	0.201	0.2382	15.62
(c)	0.208	0.2335	10.92
(d)	0.211	0.1987	5.83
(e)	0.211	0.2013	4.60
(f)	0.220	0.2359	6.74
The average error [%]			7.55

The optimization algorithm for C-PHE design compromises two output values that are as closest to the FEA simulation outputs. However, in some cases error reaches more than 10% which is a bit far from the minimum thickness of the C-PHE plate. This circumstance can be explained by the influence of the excluded design and process parameters while training the optimization algorithm. To overcome the issue, changing the input dataset by including the remaining design and process parameters such as springback phenomena to get optimal predictions would be a good practice to be followed.

Chapter 4:
Conclusions and Future Work

The AI-powered design optimization of the sheet metal forming process has gained tremendous industrial interest due to its inherent advantages, i.e., the possibility of the cost-down evaluation and the prediction of failures in shorter time compared to conventional methods. Growing interest in automotive and HVACR industries encourages the search for design optimization of the sheet metal forming process. Machine learning applications in sheet metal forming process promised affordable and robust sheet metal design methodology recently which triggered to integrate ML application to design optimization of C-PHE search. The main goal of this study was optimizing the sheet metal design and process parameters to achieve robust products with minimum cost to use in C-PHE.

To accomplish the abovementioned goal, a multilayer feed-forward neural network architecture was constructed and trained with the dataset created by using the FEA simulation of the C-PHE plate forming process. The ANN model was optimized by determining the optimum dataset separation for testing, training, and validation, and tuning the number of neurons to achieve the best accuracy for prediction. Then, a data matrix was created by using the DOE approach for the prediction of minimum thickness of the proposed sheet metals under determined design and process parameters. While the ANN model could predict the minimum thickness of the given case, the FEA simulations demonstrated approximately 7% average error in predictions. Despite the encouraging results achieved in this study, the proposed method still has several limitations such that it can be noticed that the developed ANN model contains limited design and process parameters. It would be worthwhile to explore different raw materials, different design and process parameters as input, in addition to other parameters already considered, to construct a bigger database to represent expected plate thinning amount during forming process.

BIBLIOGRAPHY

[1]D. Opritescu *et al.*, “Automated Driving by Standardizing and Scaling the Manufacturing Strategy,” *Procedia CIRP*, vol. 3, pp. 138–143, 2012, doi: 10.1016/j.procir.2012.07.025.

[2]C. Hartmann, D. Opritescu, and W. Volk, “An artificial neural network approach for tool path generation in incremental sheet metal free-forming,” *J. Intell. Manuf.*, vol. 30, no. 2, pp. 757–770, Feb. 2019, doi: 10.1007/s10845-016-1279-x.

[3]R. Shah, “Heat exchangers,” in *Bisio A, Boots SG (eds) Encyclopedia of energy technology and the environment*, John Wiley & Sons, New York, 1994, pp. 1651–1670.

[4]O. Y. Dutta and B. Nageswara Rao, “Investigations on the performance of chevron type plate heat exchangers,” *Heat Mass Transf.*, vol. 54, no. 1, pp. 227–239, Jan. 2018, doi: 10.1007/s00231-017-2107-3.

[5]J. Sodagar-Abardeh, A. Ebrahimi-Moghadam, M. Farzaneh-Gord, A. Norouzi, and Ali Norouzi, “Optimizing chevron plate heat exchangers based on the second law of thermodynamics and genetic algorithm,” *J. Therm. Anal. Calorim.*, vol. 139, no. 6, pp. 3563–3576, Mar. 2020, doi: 10.1007/s10973-019-08742-3.

[6]T.-W. Lim, Y.-S. Choi, and C.-K. Lee, “Design of plate heat exchangers for use in medium temperature organic Rankine cycles,” *Heat Mass Transf.*, vol. 55, no. 1, pp. 165–174, Jan. 2019, doi: 10.1007/s00231-018-2446-8.

[7]S. Ramesh and D. Sekulic, “Classification of heat exchangers,” in *Fundamentals of heat exchanger design*, John Wiley & Sons, Inc, 2003, pp. 25–35.

[8]J. Pilthammar, M. Schill, M. Sigvant, V. Sjöblom, and M. Lind, “Simulation of Sheet Metal Forming using Elastic Stamping Dies,” 2019.

[9]M. Dib, B. Ribeiro, and P. Prates, “Model Prediction of Defects in Sheet Metal Forming Processes,” in *Engineering Applications of Neural Networks*, E. Pimenidis and C. Jayne, Eds., in Communications in Computer and Information Science, vol. 893. Cham: Springer International Publishing, 2018, pp. 169–180. doi: 10.1007/978-3-319-98204-5_14.

[10] Q. Xu, Z. Nie, H. Xu, H. Zhou, and X.-J. Liu, “SuperMeshing: A New Deep Learning Architecture for Increasing the Mesh Density of Metal Forming Stress

Field With Attention Mechanism And Perceptual Features," *Des. Autom. Conf.*, Aug. 2021, doi: 10.1115/detc2021-71158.

[11] P. Kahhal, S. Y. A. Brooghani, and H. D. Azodi, "Multi-objective Optimization of Sheet Metal Forming Die Using Genetic Algorithm Coupled with RSM and FEA," *J. Fail. Anal. Prev.*, vol. 13, no. 6, pp. 771–778, Sep. 2013, doi: 10.1007/s11668-013-9747-5.

[12] M. H. A. Bonte, A. H. van den Boogaard, and J. Huetink, "An optimisation strategy for industrial metal forming processes," *Struct. Multidiscip. Optim.*, vol. 35, no. 6, pp. 571–586, Mar. 2008, doi: 10.1007/s00158-007-0206-3.

[13] M. H. A. Bonte, A. H. van den Boogaard, and J. Huetink, "A Metamodel Based Optimisation Algorithm for Metal Forming Processes," pp. 55–72, Jan. 2007, doi: 10.1007/3-540-69845-0_4.

[14] S. P. Leo Kumar, "State of The Art-Intense Review on Artificial Intelligence Systems Application in Process Planning and Manufacturing," *Eng. Appl. Artif. Intell.*, vol. 65, pp. 294–329, Oct. 2017, doi: 10.1016/j.engappai.2017.08.005.

[15] A. Harfoush, K. R. Haapala, and A. Tabei, "Application of Artificial Intelligence in Incremental Sheet Metal Forming: A Review," *Procedia Manuf.*, vol. 53, pp. 606–617, 2021, doi: 10.1016/j.promfg.2021.06.061.

[16] D. T. Pham and A. A. Afify, "Machine-learning techniques and their applications in manufacturing," *Proc. Inst. Mech. Eng. Part B J. Eng. Manuf.*, vol. 219, no. 5, pp. 395–412, May 2005, doi: 10.1243/095440505X32274.

[17] E. Alpaydin, *Introduction to machine learning*. in Adaptive computation and machine learning. Cambridge, Mass: MIT Press, 2004.

[18] V. Bhatnagar, S. Sharma, A. Bhatnagar, and L. Kumar, "Role of Machine Learning in Sustainable Engineering: A Review," *IOP Conf. Ser. Mater. Sci. Eng.*, vol. 1099, no. 1, p. 012036, Mar. 2021, doi: 10.1088/1757-899X/1099/1/012036.

[19] G. P. Zhang, "Neural networks for classification: a survey," *IEEE Trans. Syst. Man Cybern. Part C Appl. Rev.*, vol. 30, no. 4, pp. 451–462, Nov. 2000, doi: 10.1109/5326.897072.

[20] Y. Forghani, R. S. Tabrizi, H. S. Yazdi, and M.-R. Akbarzadeh-T, "Fuzzy support vector regression," in *2011 1st International eConference on Computer and Knowledge Engineering (ICCKE)*, Mashhad, Iran: IEEE, Oct. 2011, pp. 28–33. doi: 10.1109/ICCKE.2011.6413319.

[21] Z. Feng, W. Niu, R. Zhang, S. Wang, and C. Cheng, “Operation rule derivation of hydropower reservoir by k-means clustering method and extreme learning machine based on particle swarm optimization,” *J. Hydrol.*, vol. 576, pp. 229–238, Sep. 2019, doi: 10.1016/j.jhydrol.2019.06.045.

[22] L. J. Diamond and L. Morlino, “An Overview,” *J. Democr.*, vol. 15, no. 4, pp. 20–31, 2004, doi: 10.1353/jod.2004.0060.

[23] K. S. M. H. Ibrahim, Y. F. Huang, A. N. Ahmed, C. H. Koo, and A. El-Shafie, “A review of the hybrid artificial intelligence and optimization modelling of hydrological streamflow forecasting,” *Alex. Eng. J.*, vol. 61, no. 1, pp. 279–303, Jan. 2022, doi: 10.1016/j.aej.2021.04.100.

[24] E. Maleki, Erfan Maleki, O. Unal, M. Guagliano, and S. Bagherifard, “Analysing the Fatigue Behaviour and Residual Stress Relaxation of Gradient Nano-Structured 316L Steel Subjected to the Shot Peening via Deep Learning Approach,” *Met. Mater. Int.*, pp. 1–20, Jul. 2021, doi: 10.1007/s12540-021-00995-8.

[25] E. Maleki, O. Unal, M. Guagliano, and S. Bagherifard, “Analysing the Fatigue Behaviour and Residual Stress Relaxation of Gradient Nano-Structured 316L Steel Subjected to the Shot Peening via Deep Learning Approach,” *Met. Mater. Int.*, vol. 28, no. 1, pp. 112–131, Jan. 2022, doi: 10.1007/s12540-021-00995-8.

[26] S. Kurra, N. Hifzur Rahman, S. P. Regalla, and A. K. Gupta, “Modeling and optimization of surface roughness in single point incremental forming process,” *J. Mater. Res. Technol.*, vol. 4, no. 3, pp. 304–313, Jul. 2015, doi: 10.1016/j.jmrt.2015.01.003.

[27] J. Fürnkranz *et al.*, “Mean Squared Error,” in *Encyclopedia of Machine Learning*, C. Sammut and G. I. Webb, Eds., Boston, MA: Springer US, 2011, pp. 653–653. doi: 10.1007/978-0-387-30164-8_528.

[28] Y. Zhang and Xiaojie Xu, “Predicting springback radii and angles in air bending of high-strength sheet steel through gaussian process regressions,” *Int. J. Interact. Des. Manuf. Ijidem*, vol. 16, no. 3, pp. 863–870, Jun. 2022, doi: 10.1007/s12008-022-00945-7.

[29] X. Wu, J. Wang, A. Flitman, A. M. Flitman, and P. F. Thomson, “Neural and machine learning to the surface defect investigation in sheet metal forming,” *ICONIP99 ANZIIS99 ANNES99 ACNN99 6th Int. Conf. Neural Inf. Process. Proc. Cat No99EX378*, vol. 3, pp. 1088–1093, Nov. 1999, doi: 10.1109/iconip.1999.844687.

[30] L. Wang, M. Li, L. Zhao, and Y. Guo, “Research on a wrinkle-free forming method using low-melting alloy for sheet metal,” *Int. J. Adv. Manuf. Technol.*, vol. 99, no. 9, pp. 3065–3075, Sep. 2018, doi: 10.1007/s00170-018-2681-7.

[31] A. Shamsuzzoha, T. Kankaanpaa, Timo Kankaanpaa, Huy Nguyen, and Hoang Nguyen, “Application of machine learning algorithm in the sheet metal industry: an exploratory case study,” *Int. J. Comput. Integr. Manuf.*, pp. 1–20, Sep. 2021, doi: 10.1080/0951192x.2021.1972469.

[32] T. Qiu *et al.*, “Machine Learning Based Novelty Detection Methods for Progressive Stamping Process Health Monitoring,” 2021, doi: 10.1115/msec2020-8496.

[33] J. Henriques, “Digital twin development in metal forming: calibration aided by digital image correlation and artificial intelligence,” 2021.

[34] E. Affronti, C. Jaremenko, M. Merklein, and A. Maier, “Analysis of Forming Limits in Sheet Metal Forming with Pattern Recognition Methods. Part 1: Characterization of Onset of Necking and Expert Evaluation,” *Materials*, vol. 11, no. 9, p. 1495, Aug. 2018, doi: 10.3390/ma11091495.

[35] R. Aerens, P. Eyckens, P. Eyckens, A. Van Bael, and J. Duflou, “Force prediction for single point incremental forming deduced from experimental and FEA observations,” *Int. J. Adv. Manuf. Technol.*, vol. 46, no. 9, pp. 969–982, Feb. 2010, doi: 10.1007/s00170-009-2160-2.

[36] M. Dezelak, I. Pahole, M. Ficko, and M. Brezocnik, “MACHINE LEARNING FOR THE IMPROVEMENT OF SPRINGBACK MODELLING,” *Adv. Prod. Eng. Manag.*, vol. 7, no. 1, pp. 17–26, Mar. 2012, doi: 10.14743/apem2012.1.127.

[37] E. Georges, S. Declaye, O. Dumont, S. Quoilin, and V. Lemort, “Design of a small-scale organic Rankine cycle engine used in a solar power plant,” *Int. J. Low-Carbon Technol.*, vol. 8, no. suppl 1, pp. i34–i41, Jul. 2013, doi: 10.1093/ijlct/ctt030.

[38] O. Onal, B. Bal, D. Canadinc, and E. Akdari, “Experimental and Numerical Evaluation of Thickness Reduction in Steel Plate Heat Exchangers,” *J. Eng. Mater. Technol.*, vol. 137, no. 4, p. 041008, Oct. 2015, doi: 10.1115/1.4031080.

[39] E28 Committee, “Test Methods for Tension Testing of Metallic Materials,” ASTM International. doi: 10.1520/E0008_E0008M-13A.

[40] S. M. Hussaini, S. K. Singh, and A. K. Gupta, “Experimental and numerical investigation of formability for austenitic stainless steel 316 at elevated

temperatures," *J. Mater. Res. Technol.*, vol. 3, no. 1, pp. 17–24, Jan. 2014, doi: 10.1016/j.jmrt.2013.10.010.

[41] L. Jayahari, J. Gangadhar, S. K. Singh, and B. Balunaik, "Investigation of high temperature forming of ASS 304 using BARLAT 3-Parameter Model," *Mater. Today Proc.*, vol. 4, no. 2, pp. 799–804, 2017, doi: 10.1016/j.matpr.2017.01.088.

[42] F. Barlat *et al.*, "Plane stress yield function for aluminum alloy sheets—part 1: theory," *Int. J. Plast.*, vol. 19, no. 9, pp. 1297–1319, Sep. 2003, doi: 10.1016/S0749-6419(02)00019-0.

[43] J. LLt, "PLASTIC BEHAVIOR AND STRETCHABILITY OF SHEET METALS. PART h A YIELD FUNCTION FOR ORTHOTROPIC SHEETS UNDER PLANE STRESS CONDITIONS".

[44] D. Banabic, "Anisotropy of Sheet Metal," in *Formability of Metallic Materials*, D. Banabic, Ed., in Engineering Materials. Berlin, Heidelberg: Springer Berlin Heidelberg, 2000, pp. 119–172. doi: 10.1007/978-3-662-04013-3_4.

[45] B. Sener, E. S. Kilicarslan, and M. Firat, "Modelling Anisotropic Behavior of AISI 304 Stainless Steel Sheet Using a Fourth-Order Polynomial Yield Function," *Procedia Manuf.*, vol. 47, pp. 1456–1461, 2020, doi: 10.1016/j.promfg.2020.04.320.

[46] S. Basak, S. K. Panda, and M.-G. Lee, "Formability and fracture in deep drawing sheet metals: Extended studies for pre-strained anisotropic thin sheets," *Int. J. Mech. Sci.*, vol. 170, p. 105346, Mar. 2020, doi: 10.1016/j.ijmecsci.2019.105346.

[47] H. B. Rebelo and C. Cismaşiu, "A Comparison between Three Air Blast Simulation Techniques in LS-DYNA," 2017.

[48] T. Groensfelder, F. Giebeler, M. Geupel, D. Schneider, and R. Jaeger, "Application of machine learning procedures for mechanical system modelling: capabilities and caveats to prediction-accuracy," *Adv. Model. Simul. Eng. Sci.*, vol. 7, no. 1, p. 26, Dec. 2020, doi: 10.1186/s40323-020-00163-4.

[49] C. Kubik, M. Becker, D.-A. Molitor, and P. Groche, "Towards a systematical approach for wear detection in sheet metal forming using machine learning," *Prod. Eng.*, vol. 17, no. 1, pp. 21–36, Feb. 2023, doi: 10.1007/s11740-022-01150-x.

[50] Q. Hu, F. Zhang, X. Li, and J. Chen, "Overview on the Prediction Models for Sheet Metal Forming Failure: Necking and Ductile Fracture," *Acta Mech. Solida Sin.*, vol. 31, no. 3, pp. 259–289, Jun. 2018, doi: 10.1007/s10338-018-0026-6.

[51] X. Zhu, “Theoretical analysis of sheet metal formability,” PhD Thesis, Michigan Technological University, 1999.

[52] T. Marwala, *Finite-element-model Updating Using Computional Intelligence Techniques*. London: Springer London, 2010. doi: 10.1007/978-1-84996-323-7.

[53] T. Gro¨nsfelder, A. Hofbauer, and C. H. Richter, “A Method for Theoretical Prediction of Frequency Scatter Ranges for Freestanding Forged Steam Turbine Blades,” presented at the ASME 2011 Turbo Expo: Turbine Technical Conference and Exposition, American Society of Mechanical Engineers Digital Collection, May 2012, pp. 1085–1094. doi: 10.1115/GT2011-46172.

[54] H. Hoffmann, G. Nürnberg, K. Ersoy-Nürnberg, and G. Herrmann, “A new approach to determine the wear coefficient for wear prediction of sheet metal forming tools,” *Prod. Eng.*, vol. 1, no. 4, pp. 357–363, Nov. 2007, doi: 10.1007/s11740-007-0065-1.

[55] C. Ieracitano, A. Paviglianiti, M. Campolo, A. Hussain, E. Pasero, and F. C. Morabito, “A novel automatic classification system based on hybrid unsupervised and supervised machine learning for electrospun nanofibers,” *IEEECAA J. Autom. Sin.*, vol. 8, no. 1, pp. 64–76, Jan. 2021, doi: 10.1109/JAS.2020.1003387.

[56] A. Sharma, T. Mukhopadhyay, S. M. Rangappa, S. Siengchin, and V. Kushvaha, “Advances in computational intelligence of polymer composite materials: Machine learning assisted modeling, analysis and design”.

[57] M. Ghahramani, Y. Qiao, M. Zhou, A. OHagan, and J. Sweeney, “AI-based Modeling and Data-driven Evaluation for Smart Manufacturing Processes.” arXiv, Aug. 29, 2020. Accessed: May 23, 2023. [Online]. Available: http://arxiv.org/abs/2008.12987

[58] C. Hartmann, D. Opritescu, and W. Volk, “An artificial neural network approach for tool path generation in incremental sheet metal free-forming,” *J. Intell. Manuf.*, vol. 30, no. 2, pp. 757–770, Feb. 2019, doi: 10.1007/s10845-016-1279-x.

[59] A. Nagargoje, P. K. Kankar, P. K. Jain, and P. Tandon, “Application of artificial intelligence techniques in incremental forming: a state-of-the-art review,” *J. Intell. Manuf.*, vol. 34, no. 3, pp. 985–1002, Mar. 2023, doi: 10.1007/s10845-021-01868-y.

[60] G. Ambrogio and L. Filice, “Application of Neural Network Technique to Predict the Formability in Incremental Forming Process,” *Key Eng. Mater.*, vol. 410–411, pp. 381–389, Mar. 2009, doi: 10.4028/www.scientific.net/KEM.410-411.381.

[61] D. Opritescu and W. Volk, “Automated driving for individualized sheet metal part production—A neural network approach,” *Robot. Comput.-Integr. Manuf.*, vol. 35, pp. 144–150, Oct. 2015, doi: 10.1016/j.rcim.2015.03.006.

[62] Z. Guo and W. Tang, “Bending Angle Prediction Model Based on BPNN-Spline in Air Bending Springback Process,” *Math. Probl. Eng.*, vol. 2017, pp. 1–11, 2017, doi: 10.1155/2017/7834621.

[63] E. Hamouche and E. G. Loukaides, “Classification and selection of sheet forming processes with machine learning,” *Int. J. Comput. Integr. Manuf.*, vol. 31, no. 9, pp. 921–932, Sep. 2018, doi: 10.1080/0951192X.2018.1429668.

[64] R. Narayanasamy and P. Padmanabhan, “Comparison of regression and artificial neural network model for the prediction of springback during air bending process of interstitial free steel sheet,” *J. Intell. Manuf.*, vol. 23, no. 3, pp. 357–364, Jun. 2012, doi: 10.1007/s10845-009-0375-6.

[65] M. Levy, D. Raviv, and J. Baker, “Data Center Predictions using MATLAB Machine Learning Toolbox,” in *2019 IEEE 9th Annual Computing and Communication Workshop and Conference (CCWC)*, Las Vegas, NV, USA: IEEE, Jan. 2019, pp. 0458–0464. doi: 10.1109/CCWC.2019.8666624.

[66] S. Liu, Y. Xia, Z. Shi, H. Yu, Z. Li, and J. Lin, “Deep Learning in Sheet Metal Bending With a Novel Theory-Guided Deep Neural Network,” *IEEECAA J. Autom. Sin.*, vol. 8, no. 3, pp. 565–581, Mar. 2021, doi: 10.1109/JAS.2021.1003871.

[67] J. Xiang, T. Matsumoto, Y. Wang, and Z. Jiang, “Detect damages in conical shells using curvature mode shape and wavelet finite element method,” *Int. J. Mech. Sci.*, vol. 66, pp. 83–93, Jan. 2013, doi: 10.1016/j.ijmecsci.2012.10.010.

[68] C. Jaremenko, N. Ravikumar, E. Affronti, M. Merklein, and A. Maier, “Determination of Forming Limits in Sheet Metal Forming Using Deep Learning,” *Materials*, vol. 12, no. 7, p. 1051, Mar. 2019, doi: 10.3390/ma12071051.

[69] V. Viswanathan, B. Kinsey, and J. Cao, “Experimental Implementation of Neural Network Springback Control for Sheet Metal Forming,” *J. Eng. Mater. Technol.*, vol. 125, no. 2, pp. 141–147, Apr. 2003, doi: 10.1115/1.1555652.

[70] C.-T. Wang, G. Kinzel, and T. Altan, “Failure and wrinkling criteria and mathematical modeling of shrink and stretch flanging operations in sheet-metal forming,” *J. Mater. Process. Technol.*, vol. 53, no. 3–4, pp. 759–780, Sep. 1995, doi: 10.1016/0924-0136(94)01766-T.

[71] F.-J. Granados-Ortiz and J. Ortega-Casanova, “Machine learning-aided design optimization of a mechanical micromixer,” *Phys. Fluids*, vol. 33, no. 6, p. 063604, Jun. 2021, doi: 10.1063/5.0048771.

[72] J. Cao *et al.*, “Manufacturing of advanced smart tooling for metal forming,” *CIRP Ann.*, vol. 68, no. 2, pp. 605–628, 2019, doi: 10.1016/j.cirp.2019.05.001.

[73] M. Dib, B. Ribeiro, and P. Prates, “Model Prediction of Defects in Sheet Metal Forming Processes,” in *Engineering Applications of Neural Networks*, E. Pimenidis and C. Jayne, Eds., in Communications in Computer and Information Science, vol. 893. Cham: Springer International Publishing, 2018, pp. 169–180. doi: 10.1007/978-3-319-98204-5_14.

[74] M. S. Ashhab, T. Breitsprecher, and S. Wartzack, “Neural network based modeling and optimization of deep drawing – extrusion combined process,” *J. Intell. Manuf.*, vol. 25, no. 1, pp. 77–84, Feb. 2014, doi: 10.1007/s10845-012-0676-z.

[75] J. F. C. Khaw, B. S. Lim, and L. E. N. Lim, “Optimal design of neural networks using the Taguchi method,” *Neurocomputing*, vol. 7, no. 3, pp. 225–245, Apr. 1995, doi: 10.1016/0925-2312(94)00013-I.

[76] A. Alsamhan, A. E. Ragab, A. Dabwan, M. M. Nasr, and L. Hidri, “Prediction of formation force during single-point incremental sheet metal forming using artificial intelligence techniques,” *PLOS ONE*, vol. 14, no. 8, p. e0221341, Aug. 2019, doi: 10.1371/journal.pone.0221341.

[77] G. Ambrogio, L. Filice, F. Guerriero, R. Guido, and D. Umbrello, “Prediction of incremental sheet forming process performance by using a neural network approach,” *Int. J. Adv. Manuf. Technol.*, vol. 54, no. 9–12, pp. 921–930, Jun. 2011, doi: 10.1007/s00170-010-3011-x.

[78] S. Liu, Z. Shi, J. Lin, and Z. Li, “Reinforcement learning in free-form stamping of sheet-metals,” *Procedia Manuf.*, vol. 50, pp. 444–449, 2020, doi: 10.1016/j.promfg.2020.08.081.

[79] A. S. Gokhale, “Sheet Metal Forming in a Virtual Reality Environment using LS-DYNA and Neural N”.

[80] M. A. Dib *et al.*, "Single and ensemble classifiers for defect prediction in sheet metal forming under variability," *Neural Comput. Appl.*, vol. 32, no. 16, pp. 12335–12349, Aug. 2020, doi: 10.1007/s00521-019-04651-6.

[81] X. Liu, Y. Du, X. Lu, and S. Zhao, "Springback Prediction and Forming Accuracy Control of Micro W-bending Using Support Vector Machine," in *2019 6th International Conference on Frontiers of Industrial Engineering (ICFIE)*, London, United Kingdom: IEEE, Sep. 2019, pp. 23–27. doi: 10.1109/ICFIE.2019.8907687.

[82] N. Mekras, "Using artificial neural networks to model aluminium based sheet forming processes and tools details," *J. Phys. Conf. Ser.*, vol. 896, p. 012090, Sep. 2017, doi: 10.1088/1742-6596/896/1/012090.

Appendix A: Datasets and ML Model Outputs

Table 0.1 The training dataset for the developed ANN model.

<#>	Material Type	Cr	Ni	Mo	C	Mn	P	S	Si	N	Sheet Thickness	Strain Rate Scaling	Max Effective Surface Stress	Thinning Percentage	Minimum Thickness
		[%]	[%]	[%]	[%]	[%]	[%]	[%]	[%]	[%]	[mm]		[Mpa]	[%]	[mm]
1	316L	16.0	10	2	0.03	2	0.045	0.030	0.75	0.1	0.30	1.0	1479	30.18	0.2094
2	316L	16.0	10	2	0.03	2	0.045	0.030	0.75	0.1	0.35	1.0	1383	29.89	0.2452
3	316L	16.0	10	2	0.03	2	0.045	0.030	0.75	0.1	0.40	1.0	1300	27.75	0.2887
4	316L	16.0	10	2	0.03	2	0.045	0.030	0.75	0.1	0.45	1.0	1594	36.99	0.2813
5	316L	16.0	10	2	0.03	2	0.045	0.030	0.75	0.1	0.50	1.0	1540	26.27	0.3662
6	316L	16.0	10	2	0.03	2	0.045	0.030	0.75	0.1	0.55	1.0	1578	27.22	0.3857
7	316L	16.0	10	2	0.03	2	0.045	0.030	0.75	0.1	0.60	1.0	1571	29.74	0.4143
8	316L	16.0	10	2	0.03	2	0.045	0.030	0.75	0.1	0.65	1.0	1517	29.02	0.4535
9	316L	16.0	10	2	0.03	2	0.045	0.030	0.75	0.1	0.70	1.0	1818	29.77	0.4710
10	316L	16.0	10	2	0.03	2	0.045	0.030	0.75	0.1	0.75	1.0	1492	22.88	0.5216
11	316L	16.0	10	2	0.03	2	0.045	0.030	0.75	0.1	0.80	1.0	1352	25.12	0.5214
12	304L	17.5	8	0	0.03	2	0.045	0.015	1.00	0.1	0.30	1.0	1396	17.84	0.2465
13	304L	17.5	8	0	0.03	2	0.045	0.015	1.00	0.1	0.35	1.0	1266	15.63	0.2857

14	304L	17.5	8	0	0.03	2	0.045	0.015	1.00	0.1	0.40	1.0	1643	23.34	0.2470
15	304L	17.5	8	0	0.03	2	0.045	0.015	1.00	0.1	0.45	1.0	1640	23.40	0.2752
16	304L	17.5	8	0	0.03	2	0.045	0.015	1.00	0.1	0.50	1.0	1717	26.68	0.2688
17	304L	17.5	8	0	0.03	2	0.045	0.015	1.00	0.1	0.55	1.0	1750	35.55	0.2578
18	304L	17.5	8	0	0.03	2	0.045	0.015	1.00	0.1	0.60	1.0	1637	32.25	0.3286
19	304L	17.5	8	0	0.03	2	0.045	0.015	1.00	0.1	0.65	1.0	1551	31.37	0.4078
20	304L	17.5	8	0	0.03	2	0.045	0.015	1.00	0.1	0.70	1.0	1608	21.97	0.5017
21	304L	17.5	8	0	0.03	2	0.045	0.015	1.00	0.1	0.75	1.0	1638	22.29	0.4802
22	304L	17.5	8	0	0.03	2	0.045	0.015	1.00	0.1	0.80	1.0	1542	18.47	0.5555
23	316L	16.0	10	2	0.03	2	0.045	0.030	0.75	0.1	0.30	0.6	1473	24.62	0.2261
24	316L	16.0	10	2	0.03	2	0.045	0.030	0.75	0.1	0.35	0.6	1348	22.05	0.2728
25	316L	16.0	10	2	0.03	2	0.045	0.030	0.75	0.1	0.40	0.6	1573	23.15	0.3020
26	316L	16.0	10	2	0.03	2	0.045	0.030	0.75	0.1	0.45	0.6	1672	21.09	0.3513
27	316L	16.0	10	2	0.03	2	0.045	0.030	0.75	0.1	0.50	0.6	1809	38.32	0.3026
28	316L	16.0	10	2	0.03	2	0.045	0.030	0.75	0.1	0.55	0.6	1795	19.94	0.3615
29	316L	16.0	10	2	0.03	2	0.045	0.030	0.75	0.1	0.60	0.6	1686	29.04	0.4205
30	316L	16.0	10	2	0.03	2	0.045	0.030	0.75	0.1	0.65	0.6	1696	26.40	0.4708
31	316L	16.0	10	2	0.03	2	0.045	0.030	0.75	0.1	0.70	0.6	1715	23.76	0.5239
32	316L	16.0	10	2	0.03	2	0.045	0.030	0.75	0.1	0.75	0.6	1575	21.19	0.5343
33	316L	16.0	10	2	0.03	2	0.045	0.030	0.75	0.1	0.80	0.6	1623	19.08	0.5906
34	316L	16.0	10	2	0.03	2	0.045	0.030	0.75	0.1	0.30	0.8	1577	23.28	0.2301
35	316L	16.0	10	2	0.03	2	0.045	0.030	0.75	0.1	0.35	0.8	1318	20.53	0.2781
36	316L	16.0	10	2	0.03	2	0.045	0.030	0.75	0.1	0.40	0.8	1467	25.14	0.2981

37	316L	16.0	10	2	0.03	2	0.045	0.030	0.75	0.1	0.45	0.8	1611	23.29	0.3418
38	316L	16.0	10	2	0.03	2	0.045	0.030	0.75	0.1	0.50	0.8	1675	42.12	0.2843
39	316L	16.0	10	2	0.03	2	0.045	0.030	0.75	0.1	0.55	0.8	1880	24.19	0.2708
40	316L	16.0	10	2	0.03	2	0.045	0.030	0.75	0.1	0.60	0.8	1721	32.61	0.3958
41	316L	16.0	10	2	0.03	2	0.045	0.030	0.75	0.1	0.65	0.8	1808	33.23	0.4241
42	316L	16.0	10	2	0.03	2	0.045	0.030	0.75	0.1	0.70	0.8	2168	26.71	0.5060
43	316L	16.0	10	2	0.03	2	0.045	0.030	0.75	0.1	0.75	0.8	1825	21.16	0.5351
44	316L	16.0	10	2	0.03	2	0.045	0.030	0.75	0.1	0.80	0.8	1680	24.24	0.5665
45	304L	17.5	8	0	0.03	2	0.045	0.015	1.00	0.1	0.30	0.6	1393	19.87	0.2404
46	304L	17.5	8	0	0.03	2	0.045	0.015	1.00	0.1	0.35	0.6	1304	18.49	0.2853
47	304L	17.5	8	0	0.03	2	0.045	0.015	1.00	0.1	0.40	0.6	1451	21.85	0.3070
48	304L	17.5	8	0	0.03	2	0.045	0.015	1.00	0.1	0.45	0.6	1528	27.08	0.3259
49	304L	17.5	8	0	0.03	2	0.045	0.015	1.00	0.1	0.50	0.6	1785	26.49	0.3618
50	304L	17.5	8	0	0.03	2	0.045	0.015	1.00	0.1	0.55	0.6	1567	20.54	0.4065
51	304L	17.5	8	0	0.03	2	0.045	0.015	1.00	0.1	0.60	0.6	1816	33.53	0.3911
52	304L	17.5	8	0	0.03	2	0.045	0.015	1.00	0.1	0.65	0.6	1604	29.29	0.4508
53	304L	17.5	8	0	0.03	2	0.045	0.015	1.00	0.1	0.70	0.6	1658	23.58	0.4749
54	304L	17.5	8	0	0.03	2	0.045	0.015	1.00	0.1	0.75	0.6	1590	20.08	0.5751
55	304L	17.5	8	0	0.03	2	0.045	0.015	1.00	0.1	0.80	0.6	1653	20.48	0.5736
56	304L	17.5	8	0	0.03	2	0.045	0.015	1.00	0.1	0.30	0.8	1495	18.73	0.2417
57	304L	17.5	8	0	0.03	2	0.045	0.015	1.00	0.1	0.35	0.8	1244	16.98	0.2514
58	304L	17.5	8	0	0.03	2	0.045	0.015	1.00	0.1	0.40	0.8	1559	23.04	0.235
59	304L	17.5	8	0	0.03	2	0.045	0.015	1.00	0.1	0.45	0.8	1567	19.99	0.3559

60	304L	17.5	8	0	0.03	2	0.045	0.015	1.00	0.1	0.50	0.8	2126	17.50	0.3983
61	304L	17.5	8	0	0.03	2	0.045	0.015	1.00	0.1	0.55	0.8	1721	32.90	0.3605
62	304L	17.5	8	0	0.03	2	0.045	0.015	1.00	0.1	0.60	0.8	1844	34.57	0.3767
63	304L	17.5	8	0	0.03	2	0.045	0.015	1.00	0.1	0.65	0.8	1618	31.73	0.3980
64	304L	17.5	8	0	0.03	2	0.045	0.015	1.00	0.1	0.70	0.8	1607	28.03	0.4906
65	304L	17.5	8	0	0.03	2	0.045	0.015	1.00	0.1	0.75	0.8	1577	18.10	0.5696
66	304L	17.5	8	0	0.03	2	0.045	0.015	1.00	0.1	0.80	0.8	1593	18.18	0.5400

Table 0.2. The prediction accuracy list of developed ML models.

Regression Model	**Details**	**RMSE**	**R-Squared**	**Remarks**
Tree	Disabled PCA	6.1541	-0.14	PCA off
Linear Regression	Linear	5.5751	0.06	PCA off
Linear Regression	Interactions Linear	6.3213	-0.21	PCA off
Linear Regression	Robust Linear	5.5469	0.07	PCA off
Stepwise Linear Regression	Stepwise Linear	6.34	-0.21	PCA off
Tree	Fine Tree	6.1541	-0.14	PCA off
Tree	Medium Tree	5.4042	0.12	PCA off
Tree	Coarse Tree	5.7574	0	PCA off
SVM	Linear SVM	5.6642	0.03	PCA off
SVM	Quadratic SVM	6.0427	-0.1	PCA off
SVM	Cubic SVM	9.1768	-1.54	PCA off

SVM	Fine Gaussian SVM	5.2059	0.18	PCA off
SVM	Medium Gaussian SVM	5.2301	0.17	PCA off
SVM	Coarse Gaussian SVM	5.7098	0.02	PCA off
Ensemble	Boosted Trees	5.0211	0.24	PCA off
Ensemble	Bagged Trees	4.7882	0.31	PCA off
Gaussian Process Regression	Squared Exponential GPR	5.1429	0.2	PCA off
Gaussian Process Regression	Matern 5/2 GPR	5.1921	0.19	PCA off
Gaussian Process Regression	Exponential GPR	5.3138	0.15	PCA off
Gaussian Process Regression	Rational Quadratic GPR	5.1429	0.2	PCA off
Linear Regression	Interactions Linear	6.3213	-0.21	PCA off
Linear Regression	Linear	5.5644	0.07	PCA on
Linear Regression	Interactions Linear	5.5644	0.07	PCA on
Linear Regression	Robust Linear	5.5682	0.06	PCA on
Stepwise Linear Regression	Stepwise Linear	5.5644	0.07	PCA on
Tree	Fine Tree	6.2761	-0.19	PCA on
Tree	Medium Tree	5.578	0.06	PCA on
Tree	Coarse Tree	5.7574	0	PCA on
SVM	Linear SVM	5.671	0.03	PCA on
SVM	Quadratic SVM	5.5473	0.07	PCA on
SVM	Cubic SVM	12.407	-3.64	PCA on
SVM	Fine Gaussian SVM	5.5862	0.06	PCA on
SVM	Medium Gaussian SVM	5.5349	0.08	PCA on
SVM	Coarse Gaussian SVM	5.7386	0.01	PCA on

Ensemble	Boosted Trees	5.9448	-0.07	PCA on
Ensemble	Bagged Trees	5.6732	0.03	PCA on
Gaussian Process Regression	Squared Exponential GPR	5.3736	0.13	PCA on
Gaussian Process Regression	Matern 5/2 GPR	5.3452	0.14	PCA on
Gaussian Process Regression	Exponential GPR	5.4045	0.12	PCA on
Gaussian Process Regression	Rational Quadratic GPR	5.3421	0.14	PCA on
Neural Network	Levenberg-Marquardt	1.958699	0.951	Data Separation: Training 70% Test 15% Validation 15%
Neural Network	Bayesian Regularization	0.018222	0.977	Data Separation: Training 70% Test 15% Validation 15%
Neural Network	Scale Conjugate Gradient	2.738485	0.911	Data Separation: Training 70% Test 15% Validation 15%